Master's Thesis

MSc Smart Electrical Networks and Systems

Dynamic Analysis of a Large Scale PV Power Plants for grid support

Author: Hernan Rochina Perez

Director: Marc Cheah Mañé

Announcement: September 2019

Escola Tècnica Superior

d'Enginyeria Industrial de Barcelona

Abstract

In this report it is presented a dynamics analysis on a power plant controller considering a Photovoltaic (PV) power plant grid connection. The procedure carried out to perform this task has involved the development of grid power plant connection in pu, controllers design, linearization of non-linear model plants, grid conditions modelling and application linear control techniques. During this process it has been intended to define the power plant controller (PPC) limitations and the capabilities of a complete control structure when providing grid support. Specifically the system's response and main involved variables interaction has been investigated for different PPC time constants.

Contents

List of Figures

List of Tables

Chapter 1

Introduction

Power management in Large Photovoltaic in Power plants is not an easy task to carry out. Due to dynamic and unpredictable energy source availability plus some other technical challenges related to grid support or integration of storage systems, a system in charge of controlling the outcome of the plant is crucial. This role is played by the Power Plant controller, which behaves as a the governing system of the plant, synchronizing the performance of Voltage Source Converters (VSC), Static Synchronous Compensators (STATCOMS), capacitor banks and other components, to make the plant meet the requirements set by the Transmission System Operator in the grid's point of connection. For this reason this thesis is dedicated to the study of its operation and performance of this system in a Large Photovoltaic Power Plant.

1.1 Objectives

The study presented in this thesis project is aimed to bring insight into the performance and capabilities of a power plant controller (PPC) integrated in a simplified renewable power plant based on a voltage source converter (VSC). Knowledge on the dynamics of such system are targeted by considering different scenarios. Throughout simulations, the response limitations of a set of PI controllers that conform the PPC are explored in order to try to clarify its designed. The core objectives of this project can be summarize in the following three points:

- PPC, Active Power and Reactive power controller design for time response specifica-

tions.

- Development of linear models that represent different grid conditions: variable frequency and voltage.
- Dynamic analysis of the system considering different grid conditions and putting the focus on the PPC limitations.

1.2 Scope

The scope of this thesis is focused on the PPC speed response capabilities for some ancillary services provision. Reactive and active power supply under frequency and voltage variations in the power network are modeled and analyzed. Modeling of the generating units of the power plant and integration of multiple of them have not been considered to put emphasis on the objectives explained before.

1.3 Outline

The work and outcomes of this project are structured as follows:

- Motivation and relevant information regarding grid codes are presented in chapter 2.
- The main components of the control scheme, the study case and the different scenarios considered in this project are presented in chapter 3.
- The power plant controllers design is detailed in chapter 4.
- The development of the linear model is detailed in chapter 5.
- A validation of the controllers design and the linear model is presented in chapter 6.
- In chapter 7 results regarding the PPC dynamics are presented including time domain simulations, pole diagrams and participation factors calculation.
- Finally the conclusions are exposed in chapter 8.

Chapter 2

Renewable Energy Integration

2.1 Introduction

After the scientific community has recognised Climate Change as the main environmental issue that the human being is about to face in the near future, different strategies and policies such as Horizon 2020 and Horizon 2030 have been launched during the last years in order to reduce the effect of this phenomenon. Being CO2 emissions responsible up to great extent, the total reduction of this kind of gas emissions is needed by 2050 according to [2] to limit the global worming up to 1.5 °C. This boundary is crucial due to the irreversible effects that further warming would involve such as desserts enlargement, sea level rise, constant droughts, ecosystem loss or frequent extreme climate events.

In regard of the role that the power sector has on the emissions of CO2, it accounts for the 37% [12] of the total amount that is released considering the building and commercial, industrial, transport and the power sectors. Such impact is due to the fuel-based generating technologies that for a sustainable future are already being substituted by other technological alternatives based on renewable sources.

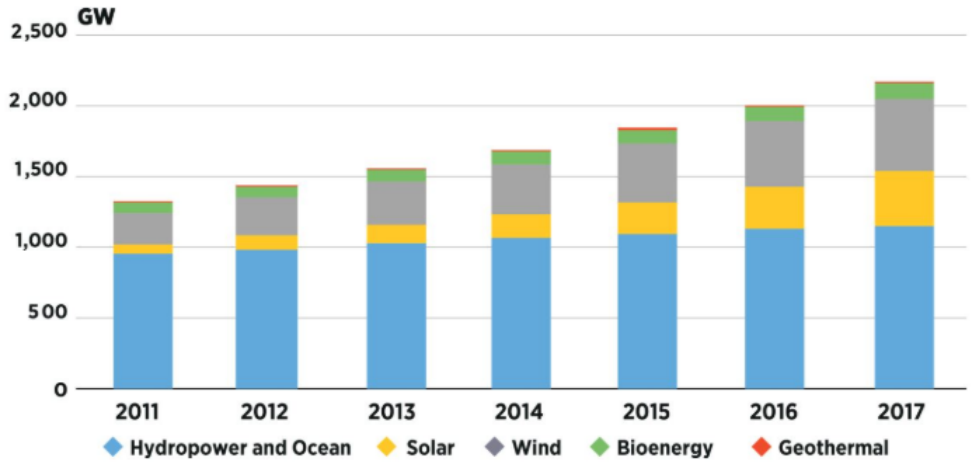

Figure 2.1: Wold's Total Renewable Power Generation Capacity per year. [10]

In Figure 2.2 the exponential growth in wind and solar capacity installation during the last years can be seen. However, it is not just the environmental point of view the key factor that has enhanced its recent rise but the truly alternative that they mean in terms of cost and reliability against conventional fossil fueled power plants. This way, renewable energy integration along energy efficiency measures are thought to have the potential to reduce the 90% of the required emissions.

On the other hand, despite renewable energy is the pathway to achieve the needed energy transition and decarbonization of the todays modern societies, this technology also involve several challenges. Unlike coal, gas or nuclear plants that can work on demand, wind and photovoltaic (PV) power plants depend on the natural source availability in every moment, which can lead to loss of supply robustness. An example on this regard is the possibility that clouds pass over a PV power plant leading to variations in the power production in that instant. It must be said though that source intermittencies are reduced when the power plant is large and the production is distributed geographically along different generating units.

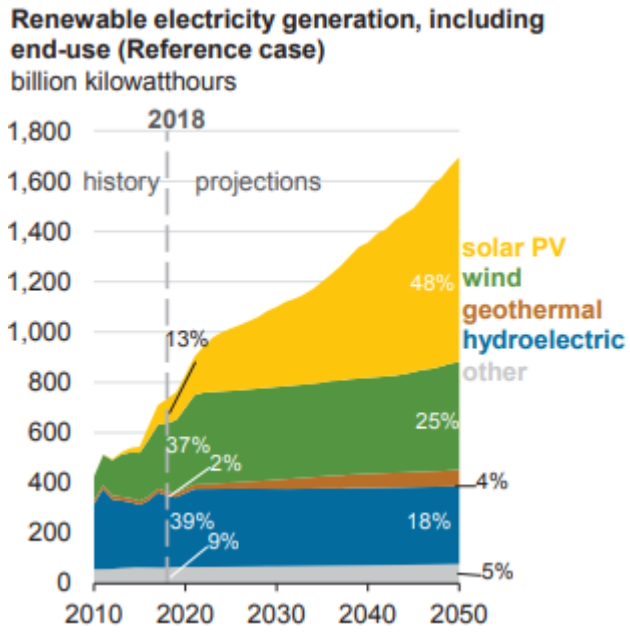

Figure 2.2: Renewable electricity generation, including end-use (Reference case). [10]

In relation to this issue, the forecast of larger capacity integration of both big power plants and smaller generating farms in the following years, is thought to be a potential threat to grids stability and reliability. To try to prevent renewable energy integration to be an issue, some territories are starting to make large renewable power plants give support to the grid. Such support is usually referred as ancillary services an their specifications are gathered in the so called Grid Codes. Besides, the grid support is fulfilled on command of the transmission system operator which give supply references to the different power plants with the aim to guarantee the reliability and safety of the supply. Further relevant topics about grid codes and large renewable power plants are presented in the following section.

2.2 Grid Codes

Due to the accelerated increase in integration of renewable energy during the last years, new grid codes have been developed to ensure stability and reliability of the power system. These new codes are focus on the lately large and very large renewable power plants installation trend. Their main purpose is to address the need of grid support. This task has been traditionally carried out by conventional plants based on synchronous generators that nowadays are being substituted by renewable large power plants due to environmental concerns. Basically, they define all compulsory requirements that at any condition the power plant needs

to fulfil, the required performance of the power plant in terms of power delivery, and when they are able to disconnect from the grid in case of variation of nominal grid conditions. This last requirement is called fault-ride through, and it specifies the minimum amount of time that the power plant must remain connected under fault conditions and the minimum amount of reactive power that needs to be injected into the grid. An example of this kind of specification can be seen in Figure 2.3, where the minimum time before possible disconnection is specified on the voltage sag level. Similar requirements also exist for over-voltages. In regard of grid frequency variation, grid codes also define requirements regarding this kind of scenarios. Example limits defined on this matter can be found in Table 2.1 for three different codes.

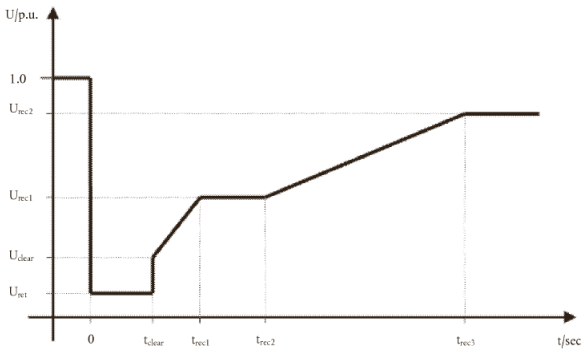

Figure 2.3: Fault-ride-through profile of a power-generating module [5]

Grid Code	Frequency (Hz)	Limits (Hz)	Maximum Duration
Germany	50	f>51.5	Instanteneous Trip
		47.5<f<51.5	Continuous
		f<47.5	Instanteneous Trip
Romania	50	f>51.5	Instanteneous Trip
		47.5<f<51.5	Continuous
		f<47.5	Instanteneous Trip
China	50	f>50.2	2 min
		49.5<f<50.2	Continuous
		48<f<49.5	10 min
		f<48	Dep. on PV Converter

Table 2.1: Frequency limits from different Grid Codes.[4]

Grid codes also classify these specifications depending on the voltage level in the point of

connection and the power capacity of the plant. Some of the requirements in terms of power that a local grid code can have are: Curtailment of active power, Primary Frequency control or droop, minimum reserves for primary frequency control,positive negative and instantaneous ramp rates, reactive power control, power factor control and voltage droop control. In the following subsection the most relevant specifications for this projects will be presented.

2.2.1 Voltage and Reactive Power Control

This requirement involves the plant capability of providing and absorbing reactive power from the grid. Such operating conditions can be given by setting different modes:reactive power set points , power factor, and voltage droop control. The first mode consist on just varying the reactive power in the point of common coupling by providing different power set-points to the power plant controller. The second operating point is defined by a power factor given by the Transport System Operator in the PCC. The voltage droop control is mechanism which sets reactive power references as a function of the voltage in the PCC, which is usually predefined by the TSO. An example of such curve can be seen in Figure 2.5, where it can be seen a dead band where the variation of voltage does not imply any reactive power reference variation, and two other regions where the voltage increase generates a reduction in the reactive power reference and viceversa.

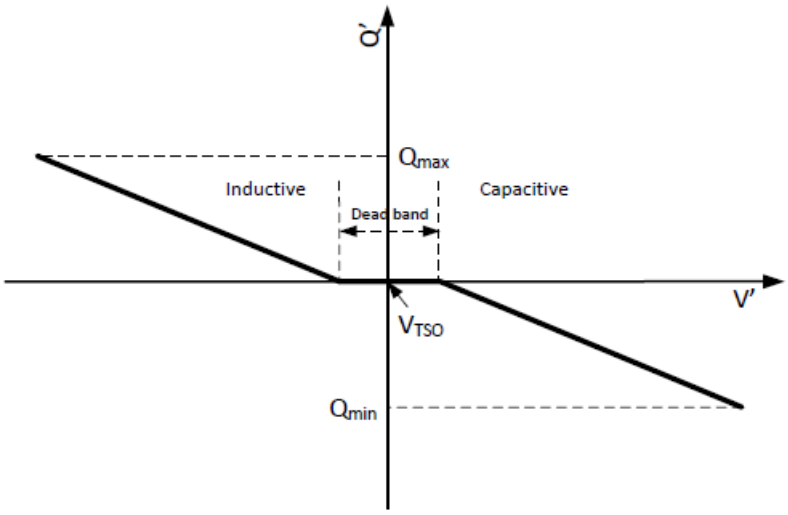

Figure 2.4: Voltage droop control [6]

2.2.2 Frequency and Active Power Control

Active power control can be undertaken on the oned hand, by means of power reference setpoints or PF relations given to the PCC by the TSO, and on the second hand through the employment of the frequency droop controls designed by the TSO. The droop control consist on the generation of active power references depending on the frequency. Usually there is range of frequencies for which the active power reference does not change, and boundary frequencies for which the droop is activated. As well, it must be point out that above, or below certain frequencies the droop control is deactivated leaving the active power reference in the minimum or maximum possible value. An example of this function can be seen below.

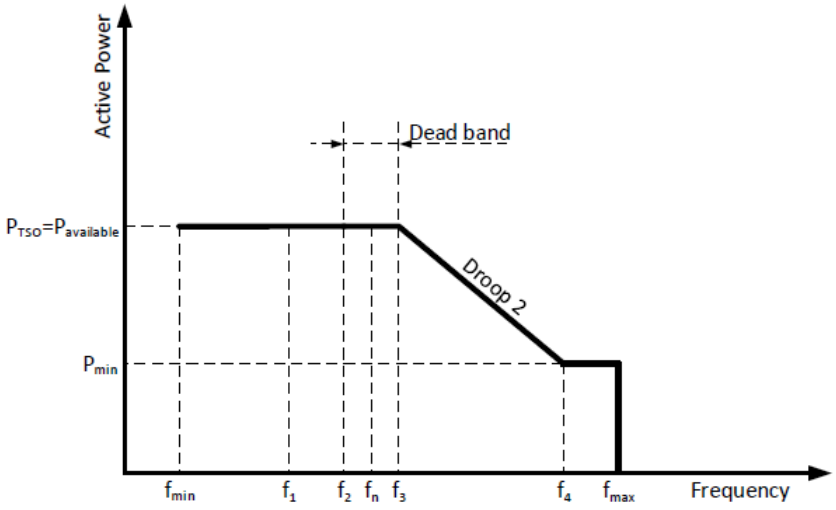

Figure 2.5: Frequency droop control [6]

Chapter 3

Plant Control Systems

3.1 Introduction

This chapter presents the different parts of the control system integrated in the plant studied and the techniques used to treat them. These subsystems are: power plant controller and the converter control system, which includes active and reactive power controller, the current controller and the phase lock loop. Such control scheme follows a cascaded topology that starts with a power reference in the PCC and eventually acts on the electrical grid by generating the required AC signals by means of the Voltage Source Converter (VSC). Due to the fundamental role of this device in the power plant, it will also briefly introduced.In relation to the methods used to deal with this control system and the electric circuits, an important point has to do with the reference frame used:the synchronous reference frame or $qd0$ frame. For this reason the power equations and the voltage equation resolutions in the $qd0$ will be first explained. After that the working principles of the different control systems are introduced. Finally, in the end of the chapter the study case of this project is detailed.

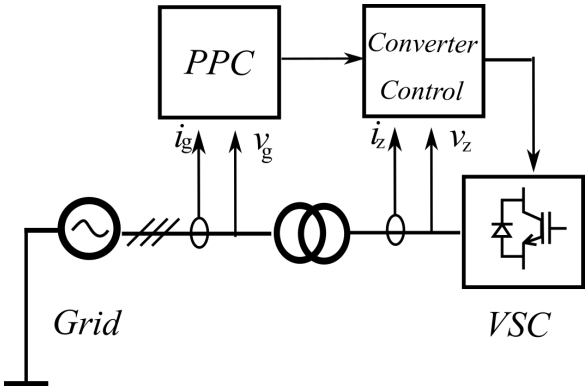

Figure 3.1: Basic Control Scheme

3.1.1 Voltage source converter

There is a wide variety of converters used in renewable energy generation. The main feature used to classify them is the semiconductor device used as switching transistor. For the case of Voltage Source Converters, this technology is usually based on Insulated-Gate Bipolar Transistors (IGBT). Some of the main advantages regarding the used of Voltage Source Converters are:

- Independent control of active and reactive power
- Black start capability
- Reduced harmonic current injection and therefore smaller filter need

The main drawback however is also related to the high switching capabilities that reduce the harmonic content but simultaneously involve an increase in power losses. On the other hand, power converters can also be classified regarding their voltage levels: Multi-level VSC and two-level VSC. For this project the two-level one is considered.

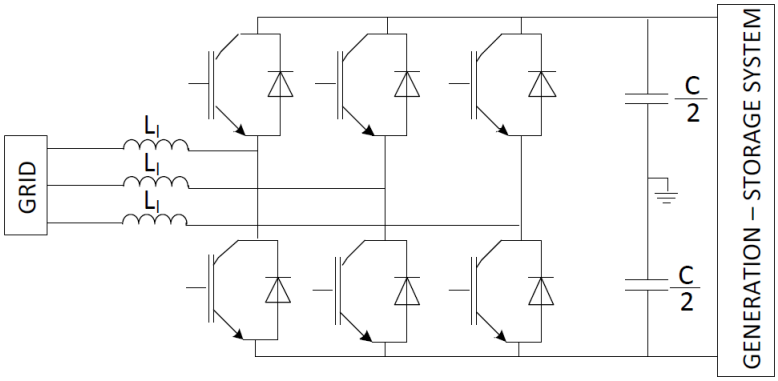

Figure 3.2: Two-Level VSC. [3]

A representative scheme of a two level converter can be found in Figure A.2. In this sketch two part can be differentiated: the right part connected to a DC source or network and the left part to an AC circuit. The working principle of this converter basically consists on the power exchange between these two sides, independently of the direction and the nature of the power, by just controlling the switches commutation that there are located in each of the three legs. Eventhough such switching commutation control is of crucial importance in real systems, for this thesis is not that relevant so that it has not been considered for the sake of computation time saving and focus on other parts of the plant control system. In this regard the alternative used is an averaged model which replaces the IGBT modules and the DC part as well. This way the VSC is substituted by a three controllable voltage sources that directly apply the required voltage calculated in the respective control units that will be explained in the following sections.

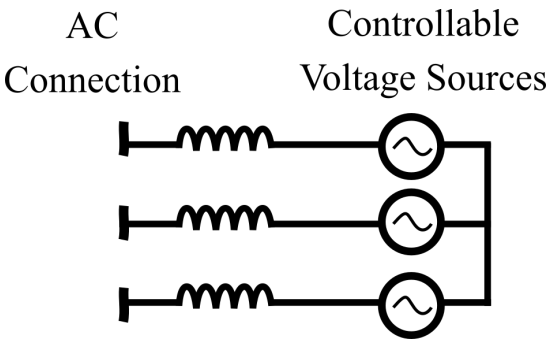

Figure 3.3: Controllable Voltage Sources

3.1.2 Power Equations in $qd0$ reference frame

Power calculations are constantly used in the model used for this project since it is the main variable to be controlled. Considering a three phase balanced system, this magnitude can be expressed as follows:

$$S = 3 \cdot V \cdot I^* = P + jQ \tag{3.1}$$

Where V is the RMS phase to neutral voltage phasor, and I is the flowing current phasor. On the other hand, the Park transformation applied to the three phase voltage and current magnitudes yield to the following phasors in the synchronous reference frame:

$$V_{qd} = \frac{v_q - jv_d}{\sqrt{2}} \tag{3.2}$$

$$I_{qd} = \frac{i_q - ji_d}{\sqrt{2}} \tag{3.3}$$

If the power equation is rewriten with the new phasors in the synchronous reference frame:

$$S = 3 \cdot V_{qd} \cdot I_{qd} = 3 \cdot \frac{v_q - jv_d}{\sqrt{2}} \frac{i_q - ji_d}{\sqrt{2}} \tag{3.4}$$

Solving the previous equation for the real part and the imaginary part leads to the active and reactive power equations in $qd0$ [16],[9]:

$$P = \frac{3}{2} \cdot (v_q \cdot i_q + v_d \cdot i_d) \tag{3.5}$$

$$Q = \frac{3}{2} \cdot (v_q \cdot i_d - v_d \cdot i_q) \tag{3.6}$$

3.1.3 Voltage equations resolution

If the circuit in Figure 3.4 is taken as an example, the voltage equation that describes the electrical behaviour of such system is deployed in Equation 3.8. $V_{z,abc}$ and $V_{l,abc}$ are considered to be balanced three phase voltage sources with no neutral connection with balanced impedances connecting them as well.

$$\begin{bmatrix} v_a^l \\ v_b^l \\ v_c^l \end{bmatrix} - \begin{bmatrix} v_a^z \\ v_b^z \\ v_c^z \end{bmatrix} = \begin{bmatrix} r_l & 0 & 0 \\ 0 & r_l & 0 \\ 0 & 0 & r_l \end{bmatrix} \begin{bmatrix} i_a \\ i_b \\ i_c \end{bmatrix} + \begin{bmatrix} l_l & 0 & 0 \\ 0 & l_l & 0 \\ 0 & 0 & l \end{bmatrix} \frac{d}{dt} \begin{bmatrix} i_a \\ i_b \\ i_c \end{bmatrix} \tag{3.7}$$

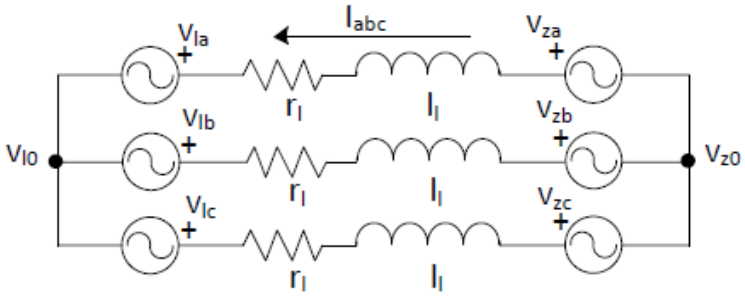

Figure 3.4: Three phase electical system

The same expression can be expressed in the synchronous reference frame by multiplying each term of the equation by the Park's rotating matrix $T(\theta)$:

$$T(\theta)v^l_{abc} - T(\theta)v^z_{abc} = T(\theta)\begin{bmatrix} r_l & 0 & 0 \\ 0 & r_l & 0 \\ 0 & 0 & r_l \end{bmatrix} i_{abc} + T(\theta)\begin{bmatrix} l_l & 0 & 0 \\ 0 & l_l & 0 \\ 0 & 0 & l_l \end{bmatrix} \frac{d}{dt} i_{abc} \tag{3.8}$$

$$v^l_{qd} - v^z_{qd} = T(\theta)\begin{bmatrix} r_l & 0 & 0 \\ 0 & r_l & 0 \\ 0 & 0 & r_l \end{bmatrix} T^{-1}(\theta) i_{qd} + T(\theta)\begin{bmatrix} l_l & 0 & 0 \\ 0 & l_l & 0 \\ 0 & 0 & l_l \end{bmatrix} \frac{d}{dt}(T^{-1}(\theta) i_{qd}) \tag{3.9}$$

$$\begin{bmatrix} v^l_q \\ v^l_d \end{bmatrix} - \begin{bmatrix} v^z_q \\ v^z_d \end{bmatrix} = \begin{bmatrix} r_l & l_l \cdot \omega \\ l_l \cdot \omega & r_l \end{bmatrix} \begin{bmatrix} i_q \\ i_d \end{bmatrix} + \begin{bmatrix} l_l & 0 \\ 0 & l_l \end{bmatrix} \frac{d}{dt} \begin{bmatrix} i_q \\ i_d \end{bmatrix} \tag{3.10}$$

Similar equations to Equation 3.10 are repeatedly applied during the the linear model assembly.

3.2 Converter Control

3.2.1 Phase Lock Loop

The phase lock loop (PLL) is a control system that is commonly used in electrical engineering applications to track the phase of a periodic signal. In this case, the PLL is used to obtain the phase of one of the V^z_{abc} voltages as it can be seen in Figure . Its role is crucial in the in-

tegration of an efficient control system based on non-alternating magnitudes since it allows the Park transformation.

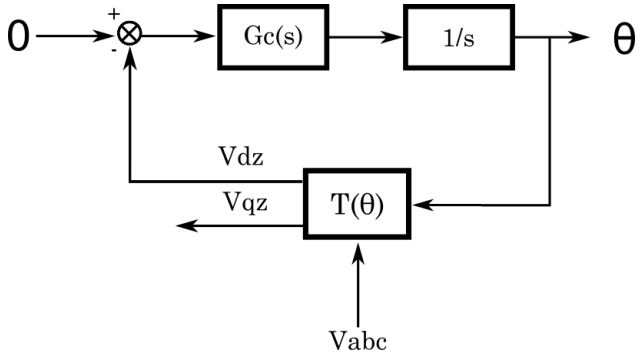

Figure 3.5: PLL control scheme.

The working principle of this control system is based on the detection of the right angular speed of the electrical magnitude that sets a input variable in the synchronous reference frame to 0.

In this case it is the magnitude V_d^z to zero, leading to an error signal that is filtered by a PI controller. The outcome of this filter is the angular speed w of the electrical magnitude used as input. After this, w is integrated resulting in the θ phase angle of the voltage that is used to calculate V_d^z and V_q^z, where V_d^z is fed back into the loop.

The design of the PI can be carried out by linearizing the system and assuming that the error in the angle detection is negligible [7]. This leads to the following transfer function:

$$\frac{\theta'(s)}{\theta(s)} = \frac{2 \cdot w_n \cdot \xi \cdot s + w_n^2}{s^2 + 2 \cdot \xi \cdot w_n^2 + w_n^2} \tag{3.11}$$

Where the ξ is the dampening ratio, w_n is the grid angular speed.

This way the PI controller has the following form:

$$Gc(s) = K_p \left(\frac{\frac{1}{\tau} + s}{s} \right) \tag{3.12}$$

Where the proportional gain is calculated as follows:

$$K_p = \frac{2\xi w_n}{V} \tag{3.13}$$

And the time constant τ:

$$\tau = \frac{2\xi}{w_n} \tag{3.14}$$

V in Equation 3.13 is the peak phase voltage where the PLL is working.

3.2.2 Current Loop

The current loop is the control system in charge of making sure that the current that flows out of the converter's terminals is the required one. For this purpose a fed-back loop system is used. An important feature of this subsystem is that it is designed to decouple the currents that in the synchronous reference frame are originally coupled. This can be seen in the voltage equation 3.15 that describes the current flow nature between two voltage sources connected by means of a inductive load (Figure 3.6).

$$\begin{bmatrix} v_q^l \\ v_d^l \end{bmatrix} - \begin{bmatrix} v_q^z \\ v_d^z \end{bmatrix} = \begin{bmatrix} r_l & l_l \cdot \omega \\ -l_l \cdot \omega & r_l \end{bmatrix} \begin{bmatrix} i_q \\ i_d \end{bmatrix} + \begin{bmatrix} l_l & 0 \\ 0 & l_l \end{bmatrix} \frac{d}{dt} \begin{bmatrix} i_q \\ i_d \end{bmatrix} \tag{3.15}$$

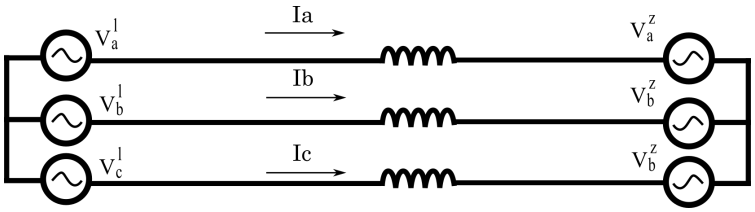

Figure 3.6: Current flow out of the converter's terminals

A representative scheme of the current loop can be seen in Figure 3.8, where the main parts are two PI controllers and a decoupling network. i_q^* and i_d^* are the current references given by the converters active and reactive power controllers while v_q^z and v_d^z are converter's voltage after the inductive filter.

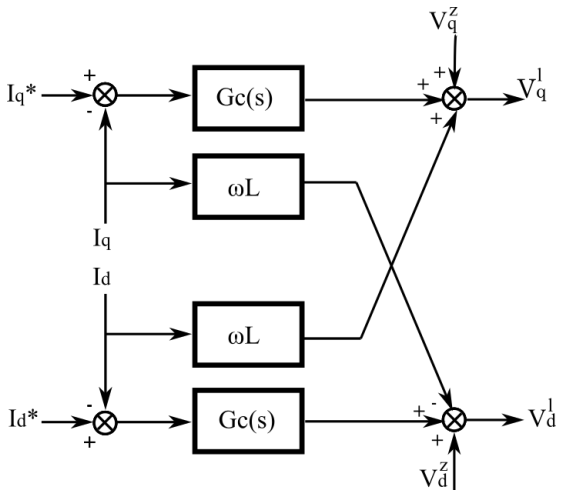

Figure 3.7: Current flow out of the converter's terminals

Finally the converter is capable of producing the desired currents by setting the outputs voltages calculated by the current controller:

$$\begin{bmatrix} v_q^l \\ v_d^l \end{bmatrix} = \begin{bmatrix} \hat{v_q^l} + v_q^z + l_l \cdot \omega \cdot i_q \\ \hat{v_d^l} + v_d^z - l_l \cdot \omega \cdot i_d \end{bmatrix} \tag{3.16}$$

Where $\hat{v_q^l}$ and $\hat{v_d^l}$ are output from the PI controllers.

3.2.3 Active and Reactive Power Control

An important part of the control of a VSC is the PQ control applied to the own converter. This system is made up of two PI controllers, which control independently the P_z active power and Q_z reactive power. These two magnitudes are controlled and measured after the inductive filter connected to the converter. Receiving a reference signal from upper layers of the plant control system, an error signal is generated. This error signal is turned into a current reference that is led to the current loop of the own converter by means of the PI controller.

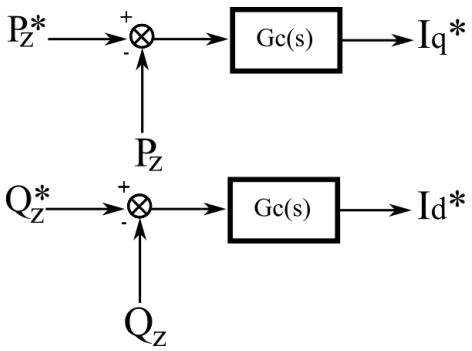

Figure 3.8: PQ converter control

When it comes to the design of the PI controllers, in order to avoid unstable behaviours of the plant it is crucial that the time constant of the studied control system is at least ten times slower than the time constant of the lower control system. This is due to the general cascaded control applied to this kind of plants. Hence, the time constant of the close-loop PQ control system will need to be designed to be ten times slower than the current loop.

3.3 Power Plant Controller

The power plant controller is the subsystem in charge of ensuring that the operating conditions follow the required power references ,P^*_{pcc} and Q^*_{pcc}, in the PCC. Its right performance and capabilities are crucial since the grid code requirements need to be fulfilled in this point. Similarly to other control subsystems integrated in the plant, two PI controllers are used to filter the error generated between the reference and the measurement for each of the variables that are intended to be tracked. The structure of the control scheme is depicted in Figure 3.9.

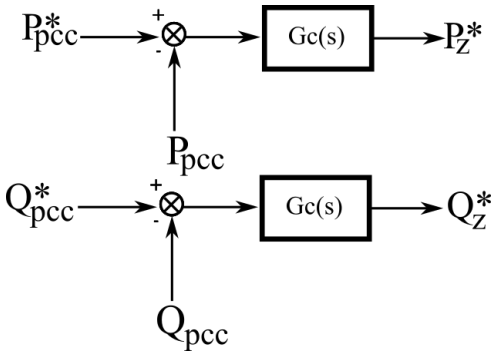

Figure 3.9: PQ converter control

On the other hand the references P^*_{pcc} and Q^*_{pcc} can be generated by many different control strategies. In the following subsections such cases are presented.

3.4 Frequency Response Model

In order to simulate frequency variations in a way as realistic as possible a model that resembles a grid frequency fluctuation has been introduced in the system studied. More specifically a model that represents the frequency variation of a thermal power plant power system based on [14].This response is not exactly the one that takes place in a common power system, but it is a simplification that can be assumed good enough in case the power system is highly populated by thermal power plants.

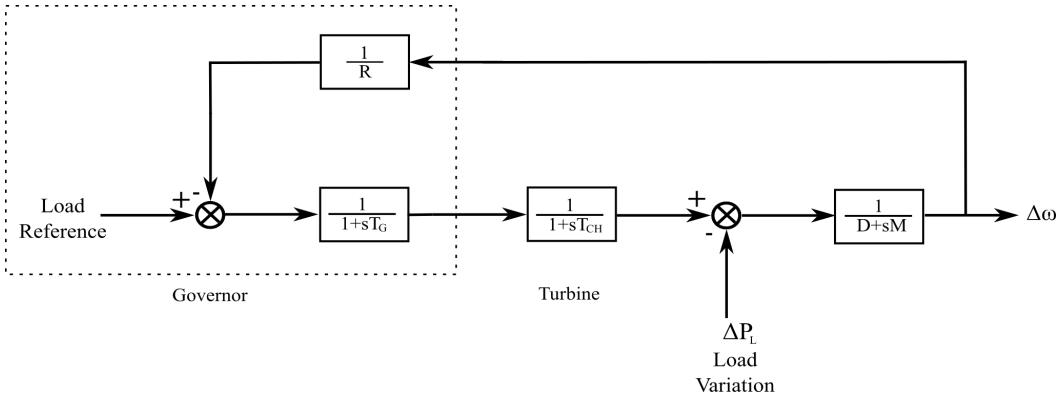

Figure 3.10: Thermal Power Plant Frequency Response Model

A representative control scheme of the varying frequency control model can be seen in Figure 3.10. This subsystem is operated by increasing the load variation from the load reference value. Since the mechanical power generation follows the load reference, this yields to a oscillating frequency decrease. In the model this variable is fed into the grid voltage sources used in the model,leading to the frequency droop control activation and the eventual modification of the active power reference in the PCC.

The study that is presented in this project is based on a simplified version of a PV power plant grid connection based on a single VSC. Although the proposed system may seem an incomplete representation of a power plant grid connection, it includes the main control elements that are implemented in a real and more complex system. For this reason it has been considered good enough to assess the PPC dynamic performance of any plant of this characterists.

3.5 Sudy Case

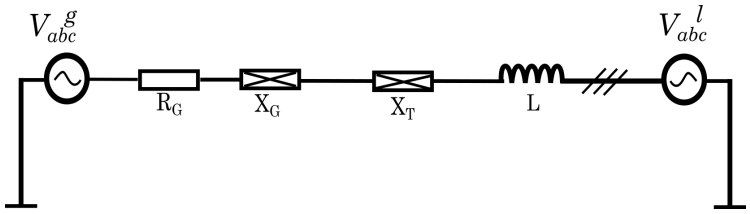

Figure 3.11: Unifilar scheme of the VSC grid connection

As it can be seen from Figure 3.11 the model is based on a three phase ideal voltage sources that represents the VSC. Such voltage sources are attached to a step-up transformer by means of an inductive filter. After the step-up transformer the point of common coupling (PCC) is found and therefore the grid connection point. This point is of crucial interest since it is where the power plant needs to fulfill all electrical requirements according to the different grid codes. The grid has been represented as a Thevening equivalent where the impedance has been calculated by means of the network's SCR.

Some of the nominal specifications of this system are the following ones:

- 1 MW nominal power rating.
- HV Line to line RMS voltage of 20 kV.
- LV Line to line RMS voltage of 400 V.

These values have taken from a real power of 3 MW.

3.5.1 Electrical Parameters

As it is common in the field of electrical engineering, the non-lineal and linear models has been defined using the per-unit system. This a very suitable and efficient way of representing electrical systems where there are different voltage levels of transformers. The base values considered for calculating each of the system's parameters are the nominal values presented previously. This magnitudes in the phase-peak form can be found in Table 3.1.

Variable	Base Value	Units
S_b	$3{\cdot}10^6$	W
$U_{b,HV}$	16330	V
$U_{b,LV}$	326	V
$I_{b,HV}$	122.4	A
$I_{b,LV}$	6123	A
$Z_{b,HV}$	133.3	Ω
$Z_{b,LV}$	0.053	Ω

Table 3.1: Base Values.

When it comes to the impedances values that build the grid connection, they can be found in Table 3.2.

Variable	Nominal Value Ω	PU Value
X_t	4	0.03
X_l	0.0106	0.2
R_l	0.0005	0.01
X_g	1.32	0.1
R_g	13.26	0.01

Table 3.2: Impedance Values.

The inductive filter values are reference values used in industry for this element. In regard of the grid impedance, it has been calculated considering a short-circuit ratio SCR of 1 by applying the equations 3.17,3.18, where S_N is the plant rated power . This value of SCR has been chosen in order to try to reach the performing limits of the system, since more common values used during a inverter's desing are around 10 [8].

$$Z_g = \frac{V_N^2}{S_N \cdot SCR} \tag{3.17}$$

$$\frac{X_g}{R_g} = 10 \tag{3.18}$$

On the other side, the transformers impedance has been obtained considering a series reac-

tance x_t with a value equal to 5% of the transformer's nominal power:

$$X_t = x_t \cdot \frac{V_N^2}{S_N} \tag{3.19}$$

Apart from this, some changes need to be applied to the converter to grid connection equations in order to set a model in which all the variables are in pu system but time. This is very important due to the dynamic caracter of the simulations that are going to be carried out for this thesis. According to [1], this can be figured out just by multiplying every time derivative times $1/w_b$. If a voltage drop is considered as example, such transformation can easily be seen from Equation 3.20 to 3.21

$$v_q^{l,g} - v_q^{g,g} = (R_l + R_g) \cdot i_q^g + (L_l + L_g + L_t) \cdot \frac{di_q^g}{dt} + (L_l + L_g + L_t) \cdot \omega \cdot i_d^g \tag{3.20}$$

$$v_q^{l,g} - v_q^{g,g} = (R_l + R_g) \cdot i_q^g + \frac{(L_l + L_g + L_t)}{\omega_b} \cdot \frac{di_q^g}{dt} + (L_l + L_g + L_t) \cdot \omega \cdot i_d^g \tag{3.21}$$

3.5.2 Study Strategy

As it has been said before, the PPC can be set to follow several control modes of active and reactive power in the point of common coupling. In this regard, the following subsections introduce the different cases that are going to be considered during this project with the aim of analysing the plant performance when different control modes are applied.

Case 1: P^*_{pcc}/Q^*_{pcc} setpoint variation

This control mode consists on directly giving reference steps of active power to the power plant controller. In addition, a constant power factor of $cos(\phi_{pcc})$=0.95 is intended to be maintained at every moment on the PCC . This way in case of any P^*_{pcc} variation a new reactive power reference is given according to the following expression:

$$Q^*_{pcc} = P_{pcc} \cdot tan(\phi_{pcc}) \tag{3.22}$$

Case 2: Frequency droop control

In this case, the active power setpoint is calculated as a function of the measured frequency in the grid. This control strategy is called frequency droop control and an example of how it is applied can be seen in Figure 2.5.

For simulating this case, the models will be run at the limiting frequency prior the actuation of the frequency droop control, i.e. f3 when comparing to the plot of Figure 2.5. At this point a frequency change is simulated according to the description give in subsection 3.4. As a result of the frequency droop opearation and active power reference variation takes place. On the other hand, Q^*_{pcc} will simultaneously follow the varying P^*_{pcc} keeping the relation Q^*_{pcc}=$P_{pcc} \cdot tan(\phi_{pcc})$. The value considered for the droop slope is K_f=-0.47 [6].

Case 3: V^{pcc} droop control of Q^*_{pcc}

Similarly to the previous case, Q^*_{pcc} is generated as a function of the variation of V^{pcc}. This control mode is the so-called voltage droop control and works measuring the voltage variation in the PCC. As a result of the droop actuation Q^*_{pcc} is proportionally adjusted to the slope of the droop curve considered. Such voltage variation is modeled by simulating a symmetric voltage sag in the grid. The same way as in the other cases the power factor is kept in the PCC by adjusting P^*_{pcc} . It must be said though that the common use of PF control aims to adjust Q^*_{pcc} going after P^*_{pcc} variations. In this project the slope of the droop has been taken from [6] with a value of $K_v = -0.5$.

Chapter 4

Controllers Design

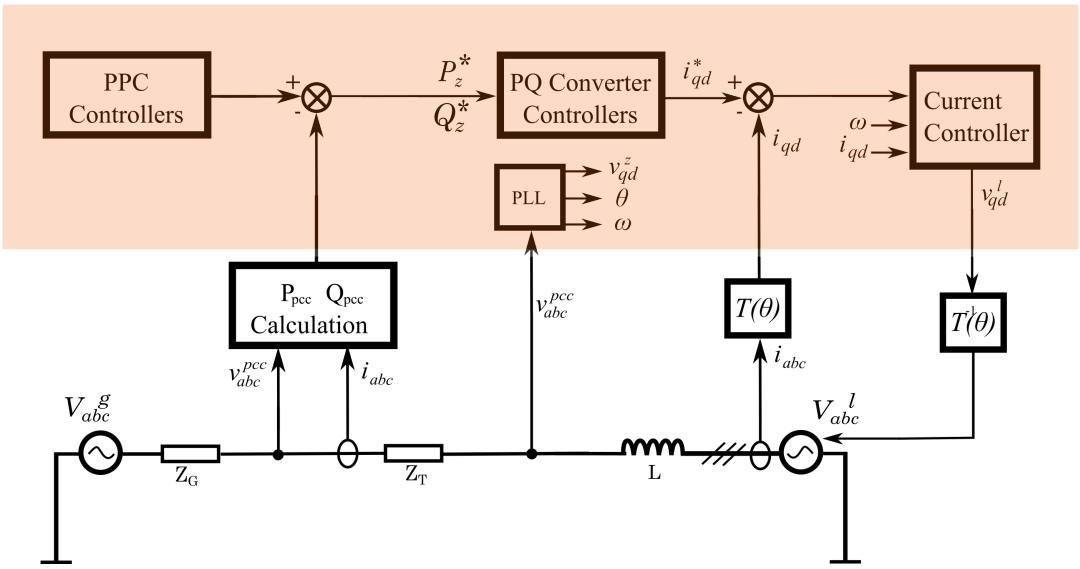

Figure 4.1: Unifilar scheme of the VSC grid connection

Apart from the electrical parameters the plant performance is as well highly influenced by the control parameters that are found in the different plant controllers. As it can be seen in Figure 4.1, there is a total of four control systems. Each of them is made up of two PI controllers but the PLL, where there is just one implemented. In this section the design of each of this controllers by means of the Internal Mode Control theory is explained as well as the values of its parameters.

4.0.1 Current Controller Design

Due to the decoupling network in the current loop the transfer functions for the currents are:

$$\frac{i_q(s)}{v_q^l(s)} = G_{i_d}(s) = \frac{1}{\frac{L_l}{w_b} \cdot s + R_l} \tag{4.1}$$

$$\frac{i_d(s)}{v_d^l(s)} = G_{i_q}(s) = \frac{1}{\frac{L_l}{w_b} \cdot s + R_l} \tag{4.2}$$

Now,by setting the closed loops current dynamics follow a first order system such as the one defined in Equations 4.3 and 4.4, a PI cotroller $C(s)$ can be calculated according to the fed-back closed loop transfer function expression as it can be seen in 4.5:

$$G_{c,iq}(s) = \frac{i_d(s)}{i_d^*(s)} = \frac{1}{\tau_i s + 1} \tag{4.3}$$

$$G_{c,id}(s) = \frac{i_q(s)}{i_q^*(s)} = \frac{1}{\tau_i s + 1} \tag{4.4}$$

$$C(s) = \frac{1}{G(s)} \frac{G_c(s)}{1 - G_c(s)} \tag{4.5}$$

By substituting $G_c(s)$ and $G(s)$ in Equation 4.5, the PI controller results in the following transfer function:

$$C_i(s) = \frac{L_l \cdot}{\tau} + \frac{R_l \cdot}{\tau s} = K_{p,i} + \frac{K_{i,i}}{s} \tag{4.6}$$

Something to remark about these PI controllers design is that both for i_q and i_d the proportional and integral gains have the same values since L_l, R_l and τ are equal for the two cases. Such parameters can be found in Table 4.1.

$K_{p,i}$	10
$K_{i,i}$	50
τ_i	0.001s

Table 4.1: Current Controller Parameters

When it comes to the time constant considered, 1 ms is the most common value considered for this kind of applications.

4.0.2 Converter Controller Design

A similar approach is considered for the design of the converter controller. In this case it is also set that the P_z and Q_z closed loops follow first order system dynamics but with a higher time constant, $\tau_z >> \tau_i$.

$$G_{c,Pz}(s) = \frac{P_z(s)}{P_z^*(s)} = \frac{1}{\tau_z s + 1} \tag{4.7}$$

$$G_{c,Qz}(s) = \frac{Q_z(s)}{Q_z^*(s)} = \frac{1}{\tau_z s + 1} \tag{4.8}$$

Besides, the transfer functions considered for $P_z(s)$ and $Q_z(s)$ are the following ones:

$$\frac{P_z(s)}{i_q^*(s)} = G_{P_z}(s) = \frac{3/2 \cdot v_q^z}{\tau_i \cdot s + 1} \tag{4.9}$$

$$\frac{Q_z(s)}{i_d^*(s)} = G_{Q_z}(s) = \frac{3/2 \cdot v_q^z}{\tau_i \cdot s + 1} \tag{4.10}$$

The transfer functions presented are a result of the cascaded control that links the converter controller output with the current loop controller input.

On the one hand the plant considered keep the time constant chosen for the currents transfer functions for two reasons: it is considered that the power mainly depends on the current and that the current closed loop is much faster than the power closed loops.

On the other hand the gain is calculated considering the instantaneous power equations in qd with the following approximationns: the difference between the current reference and the current measurement is negligible, v_d^z is negligible due to the PLL setting, and last the variation in v_q^z is negligible during the power plant operation in addition to the fact that it is not considered the main variable that influences on the power but the current.

$$P_z(t) \approx \frac{3}{2} v_q^z \cdot i_q^*(t)$$

$$Q_z(t) \approx \frac{3}{2} v_q^z \cdot i_d^*(t)$$

If equation 4.5 is applied again solving with the plant transfer function and the closed loop

transfer function, the PI controller obtained is the next one:

$$C_z(s) = \frac{\tau_i}{\tau_z \cdot 3/2 \cdot v_q^z} + \frac{1}{\tau_z \cdot 3/2 \cdot v_q^z \cdot s} = K_p + \frac{K_i}{s} \tag{4.11}$$

The values of the PI parameters for P_z Q_z are shown in Table 4.2. Something to remark about τ_i is that even if a much smaller could have been chosen, this is a value based on industrial practice.

$K_{p,z}$	0.005227
$K_{i,z}$	5.227
τ_i	0.15 s

Table 4.2: Current Controller Parameters

4.0.3 Power Plant Controller Design

The strategy followed to design the PPC PI constollers is the same as the previous ones: considering first order closed-loop dynamics with a time constant higher than the one from the following controller.

$$G_{c,Ppcc}(s) = \frac{P_{pcc}(s)}{P^*_{pcc}(s)} = \frac{1}{\tau_z s + 1} \tag{4.12}$$

$$G_{c,Qpcc}(s) = \frac{Q_{pcc}(s)}{Q^*_{pcc}(s)} = \frac{1}{\tau_{pcc} s + 1} \tag{4.13}$$

When it comes to the plant transfer functions for the active and reactive power in the point of common coupling, they have been defined considering as input variables $P^*_z(s)$ and $Q^*_z(s)$ since they are the output from the PPC into the next cascaded controller.

$$\frac{P_{pcc}(s)}{P^*_z(s)} = G_{P_{pcc}}(s) = \frac{K_{Ppcc}}{\tau_z \cdot s + 1} \tag{4.14}$$

$$\frac{Q_{pcc}(s)}{Q^*_z(s)} = G_{Q_{pcc}}(s) = \frac{K_{Qpcc}}{\tau_z \cdot s + 1} \tag{4.15}$$

When it comes to the gains of the transfer functions in 4.14 and 4.15, they have been calculation as a relation of the voltage and power factors in the filter terminals and the point of common coupling:

$$K_{Ppcc} = \frac{V^{pcc} \cdot cos(\phi_{pcc})}{V^{z} \cdot cos(\phi_{z})} \tag{4.16}$$

$$K_{Qpcc} = \frac{V^{pcc} \cdot sin(\phi_{pcc})}{V^{z} \cdot sin(\phi_{z})} \tag{4.17}$$

This gains are thought to turn a converter power reference in a current (dividing in the denominator), that at the same time become a power magnitude in the PCC (multiplying times the numerator). Of course, this parameter tuning is very influenced by the plant topology presented in this project, but similar proposals could be used for other plants.

This way using equation 4.5 the PI controllers for P_{pcc} and Q_{pcc} result in:

$$C_{Ppcc}(s) = \frac{\tau_z}{\tau_{pcc} \cdot K_{Ppcc}} + \frac{1}{\tau_{pcc} \cdot K_{Ppcc}} = K_{p,Pcc} + \frac{K_{p,Qpcc}}{s} \tag{4.18}$$

$$C_{Qpcc}(s) = \frac{\tau_z}{\tau_{pcc} \cdot K_{Qpcc}} + \frac{1}{\tau_{pcc} \cdot K_{Qpcc}} = K_{p,Qpcc} + \frac{K_{i,Qpcc}}{s} \tag{4.19}$$

The values used in the PI parameters can be found below. However it must be remarked that this are the starting values used for building the linear model. From this value, the time constant will be decreased aiming faster responses.

$K_{p,Ppcc}$	0.15
$K_{i,Ppcc}$	1
$K_{p,Qpcc}$	0.203
$K_{i,Qpcc}$	1.358
τ_i	1s

Table 4.3: Power Plant Controller Parameter

Chapter 5

Linear Model

5.1 Introduction

After defining the non-linear model the next step required for studying the stability and performance limitations of the system considered is obtaining a linear model based on the previous non-linear model. This linear model is possible to be built in a State Space form that will allow to control the input references and visualize the different variable outcomes. The form it is usually expressed is as shown in Equations 5.1 and 5.2. In those expressions X is a vector of the system states, and U and Y, the vector of incomes and the outcomes of the system respectively.

$$\dot{X} = AX + BU \tag{5.1}$$

$$Y = CX + DU \tag{5.2}$$

According to the purpose of this chapter, the linearization process is explained during the first section. After that, the following sections show step by step how this linear model has been built for each part of the system, including for each of them: the linearization carried out if needed, its state space form pointing out each of the state space matrices and variables. Afterwards, a representative block diagram of the whole system is also presented before finally introducing the control linear techniques used to analyze the system are presented.

5.1.1 Linearization

This process consists on replacing a non-linear function by a linear approximation of it. In order to obtain that approximated function a first order Taylor series of the non-linear function has been used:

$$f(x) \approx f(a) + f'(a) \cdot (x - a) + R \tag{5.3}$$

The previous expression basically points that the value of the non-linear function f in a certain point x is close to the value of the non-linear function in a previous equilibrium point, a, plus its time derivative times the difference from the equilibrium point where the function is evaluated now. Therefore an equilibrium point is always needed to build a linear model so that everytime a new linear model is wanted to be built, a set of equilibrium points will be extracted from a non-linear model simulation.

5.2 Small Signal Model

5.2.1 Grid connection

This subsection focuses on the equations that describe the voltage drop between the converter, V^l_{abc} and the grid, V^g_{abc}, both in its standard and linearized forms. Apart from this the state space matrices of the subsystem are presented point out the inputs,outputs and states.

Non-linear equations:

$$v_q^{l,g} - v_q^{g,g} = (R_l + R_g) \cdot i_q^g + \frac{(L_l + L_g + L_t)}{\omega_b} \cdot \frac{di_q^g}{dt} + (L_l + L_g + L_t) \cdot \omega \cdot i_d^g \tag{5.4}$$

$$v_d^{l,g} - v_d^{g,g} = (R_l + R_g) \cdot i_d^g + \frac{(L_l + L_g + L_t)}{\omega_b} \cdot \frac{di_d^g}{dt} - (L_l + L_g + L_t) \cdot \omega \cdot i_q^g \tag{5.5}$$

$$v_q^{z,g} - v_q^{g,g} = R_l \cdot i_q^g + \frac{(L_l)}{\omega_b} \cdot \frac{di_q^g}{dt} + L_l \cdot \omega \cdot i_d^g \tag{5.6}$$

$$v_d^{z,g} - v_d^{g,g} = R_l \cdot i_d^g + \frac{(L_l)}{\omega_b} \cdot \frac{di_d^g}{dt} - L_l \cdot \omega \cdot i_q^g \tag{5.7}$$

$$v_q^{pcc,g} - v_q^{g,g} = R_l \cdot i_q^g + \frac{(L_l + L_t)}{\omega_b} \cdot \frac{di_q^g}{dt} + (L_l + L_t) \cdot \omega \cdot i_d^g \tag{5.8}$$

$$v_d^{pcc,g} - v_d^{g,g} = R_l \cdot i_d^g + \frac{(L_l + L_t)}{\omega_b} \cdot \frac{di_d^g}{dt} - (L_l + L_t) \cdot \omega \cdot i_q^g \tag{5.9}$$

Linearized equations of the subsytem:

$$v_q^{l,g} - v_q^{g,g} = (R_l + R_g) \cdot i_q^g + \frac{(L_l + L_g + L_t)}{\omega_b} \cdot \frac{di_q^g}{dt} + (L_l + L_g + L_t) \cdot (\omega \cdot i_{d0}^g + \omega_0 \cdot i_d^g) \tag{5.10}$$

$$v_d^{l,g} - v_d^{g,g} = (R_l + R_g) \cdot i_d^g + \frac{(L_l + L_g + L_t)}{\omega_b} \cdot \frac{di_d^g}{dt} - (L_l + L_g + L_t) \cdot (\omega \cdot i_{q0}^g + \omega_0 \cdot i_q^g) \tag{5.11}$$

$$v_q^{z,g} - v_q^{g,g} = R_l \cdot i_q^g + \frac{(L_l)}{\omega_b} \cdot \frac{di_q^g}{dt} + L_l \cdot (\omega \cdot i_{d0}^g + \omega_0 \cdot i_d^g) \tag{5.12}$$

$$v_d^{z,g} - v_d^{g,g} = R_l \cdot i_d^g + \frac{(L_l)}{\omega_b} \cdot \frac{di_d^g}{dt} - L_l(\omega \cdot i_{q0}^g + \omega_0 \cdot i_q^g) \tag{5.13}$$

$$v_q^{pcc,g} - v_q^{g,g} = R_l \cdot i_q^g + \frac{(L_l + L_t)}{\omega_b} \cdot \frac{di_q^g}{dt} + (L_l + L_t)(\omega \cdot i_{d0}^g + \omega_0 \cdot i_d^g) \tag{5.14}$$

$$v_d^{pcc,g} - v_d^{g,g} = R_l \cdot i_d^g + \frac{(L_l + L_t)}{\omega_b} \cdot \frac{di_d^g}{dt} - (L_l + L_t)(\omega \cdot i_{q0}^g + \omega_0 \cdot i_q^g) \tag{5.15}$$

Comparing the two subsets of equations it can be seen that the main difference is the linearization of the multiplication of the currents i_q,i_d and the grids angular's speed ω. This operation is essential in the linear model validation due the variable ω considered in this study. The state form of these subsystem of equations can be found below with the matrices A, B, C, D as well as the inputs u, states x and outputs y.

$$\mathrm{A} = \begin{bmatrix} \dfrac{-\omega \cdot (R_l + R_g)}{(L_l + L_g + L_t)} & -\omega \\ \omega & \dfrac{-\omega \cdot (R_l + R_g)}{(L_l + L_g + L_t)} \end{bmatrix}$$

$$B = \begin{bmatrix} \dfrac{\omega}{(L_l + L_g + L_t)} & 0 & \dfrac{-\omega}{(L_l + L_g + L_t)} & 0 & -\omega \cdot i_{d0} \\ 0 & \dfrac{\omega}{(L_l + L_g + L_t)} & 0 & \dfrac{-\omega}{(L_l + L_g + L_t)} & \omega \cdot i_{q0} \end{bmatrix}$$

$$C = \begin{bmatrix} 1 & 0 \\ 0 & 1 \\ \dfrac{-L_g \cdot R_l + L_l \cdot R_g + L_t \cdot R_g}{(L_l + L_g + L_t)} & 0 \\ 0 & \dfrac{-L_g \cdot R_l + L_l \cdot R_g + L_t \cdot R_g}{(L_l + L_g + L_t)} \\ \dfrac{-L_g \cdot R_l + L_l \cdot R_g - L_t \cdot R_g}{(L_l + L_g + L_t)} & 0 \\ 0 & \dfrac{-L_g \cdot R_l + L_l \cdot R_g - L_t \cdot R_g}{(L_l + L_g + L_t)} \end{bmatrix}$$

$$D = \begin{bmatrix} 0 & 0 & 0 & 0 & 0 \\ 0 & 0 & 0 & 0 & 0 \\ \dfrac{L_g}{(L_l + L_g + L_t)} & 0 & \dfrac{L_l + L_t}{(L_l + L_g + L_t)} & 0 & 0 \\ 0 & \dfrac{L_g}{(L_l + L_g + L_t)} & 0 & \dfrac{L_l + L_t}{(L_l + L_g + L_t)} & 0 \\ \dfrac{L_g + L_t}{(L_l + L_g + L_t)} & 0 & \dfrac{L_l}{(L_l + L_g + L_t)} & 0 & 0 \\ 0 & \dfrac{L_g + L_t}{(L_l + L_g + L_t)} & 0 & \dfrac{L_l}{(L_l + L_g + L_t)} & 0 \end{bmatrix}$$

$$u = \{\Delta\omega_g, \Delta u_q^{l,g}, \Delta u_d^{l,g}, \Delta u_q^{g,g}, \Delta u_d^{g,g}\}$$

$$x = \{\Delta i_q^g, \Delta i_d^g\}$$

$$y = \{\Delta i_q^g, \Delta i_d^g \Delta u_q^{pcc,g}, \Delta u_d^{pcc,g} \Delta u_q^{z,g}, \Delta u_d^{z,g}\}$$

Finally this state space subsystem can be graphically presented as the block shown in Figure 5.1:

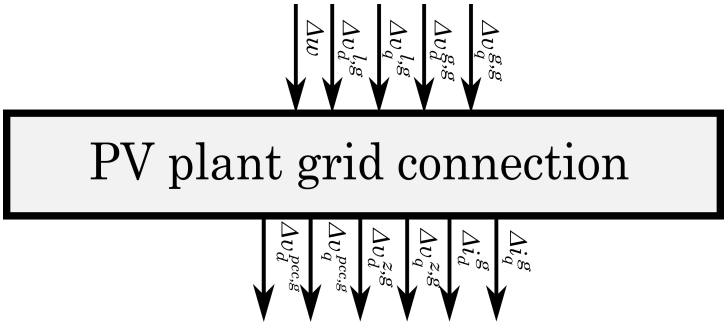

Figure 5.1: Grid Connection Block

5.2.2 Current Loop

The mathematical model of the current loop includes two equations each of them for controlling the q and d component of the current and two more equations for computing the error from the current references:

$$e_{i_q} = i_q^{*,pll} - i_q^{pll}$$

$$e_{i_d} = i_d^{*,pll} - i_d^{pll}$$

The non-linear equations:

$$v_q^{l,pll} = e_{i_q} \cdot (k_{p,cl} + \int k_{i,cl} \cdot dt) + v_q^{z,pll} - \omega_{pll} \cdot i_d^{pll} \tag{5.16}$$

$$v_d^{l,pll} = e_{i_d} \cdot (k_{p,cl} + \int k_{i,cl} \cdot dt) + v_d^{z,pll} - \omega_{pll} \cdot i_q^{pll} \tag{5.17}$$

The linear equatios:

$$v_q^{l,pll} = e_{i_q} \cdot (k_{p,cl} + \int k_{i,cl} \cdot dt) + v_q^{z,pll} + (\omega_{pll,0} \cdot i_d^{pll} + \omega_{pll} \cdot i_{d,0}^{pll}) \tag{5.18}$$

$$v_d^{l,pll} = e_{i_d} \cdot (k_{p,cl} + \int k_{i,cl} \cdot dt) + v_d^{z,pll} - (\omega_{pll,0} \cdot i_q^{pll} + \omega_{pll} \cdot i_{q,0}^{pll}) \tag{5.19}$$

The same way as in the previous example, the linearization carried out in the subsystem just affects the product between the angular's speed measured by the PLL and the currents. The state space elements that define this subsystem can be found below as well as its block diagram.

$$A = \begin{bmatrix} 0 & 0 \\ 0 & 0 \end{bmatrix}$$

$$B = \begin{bmatrix} 1 & 0 & 0 & 0 & 0 & 0 & 0 \\ 0 & 1 & 0 & 0 & 0 & 0 & 0 \end{bmatrix}$$

$$C = \begin{bmatrix} k_{i,cl} & 0 \\ 0 & k_{i,cl} \end{bmatrix}$$

$$D = \begin{bmatrix} k_{p,cl} & 0 & 0 & \omega_{pll,0} \cdot L_l & 1 & 0 & i_{d,0} \cdot L_l \\ 0 & k_{p,cl} & -\omega_{pll,0} \cdot L_l & 0 & 0 & 1 & -i_{q,0} \cdot L_l \end{bmatrix}$$

$$u = \{\Delta e_{i_q}, \Delta e_{i_d}, \Delta i_q^{pll}, \Delta i_d^{pll}, \Delta u_q^{z,pll}, \Delta u_d^{z,pll}, \Delta w_{pll}\}\ x = \{\Delta E_{i_q}, \Delta E_{i_d}\}\ y = \{\Delta u_q^{l,pll}, \Delta u_d^{l,pll}\}$$

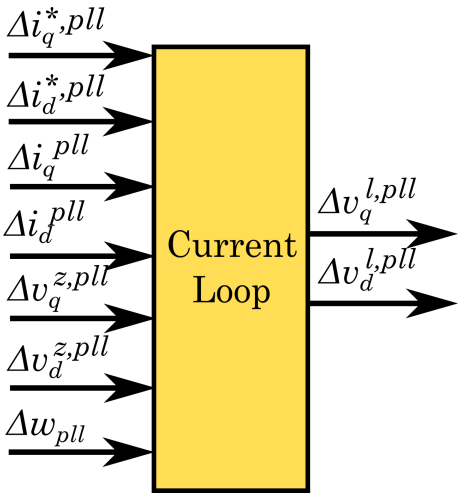

Figure 5.2: Current Loop Block

5.2.3 Converter Active and Reactive Power Control

This subsystem is based on two PI controllers that supervise the active and reactive power output of the VSC by setting current references. This controllers act on the error between the reference and the power measurement.

$$e_{P_z} = P_z^* - P_z$$

$$e_{Q_z} = Q_z^* - Q_z$$

$$i_q^{*,pll} = e_{P_z} \cdot (k_{p,P_z} + \int k_{i,P_z} \cdot dt) \tag{5.20}$$

$$i_d^{*,pll} = e_{Q_z} \cdot (k_{p,Q_z} + \int k_{i,Q_z} \cdot dt) \tag{5.21}$$

$$A = \begin{bmatrix} 0 & 0 \\ 0 & 0 \end{bmatrix}$$

$$B = \begin{bmatrix} 1 & 0 \\ 0 & 1 \end{bmatrix}$$

$$C = \begin{bmatrix} k_{i,P_z} & 0 \\ 0 & k_{i,Q_z} \end{bmatrix}$$

$$D = \begin{bmatrix} k_{p,P_z} & 0 \\ 0 & k_{p,Q_z} \end{bmatrix}$$

$$u = \{\Delta e_{P_z}, \Delta e_{Q_z}\}$$

$$x = \{\Delta E_{P_z}, \Delta E_{Q_z}\}$$

$$y = \{\Delta i_q^{*,pll}, \Delta i_d^{*,pll}\}$$

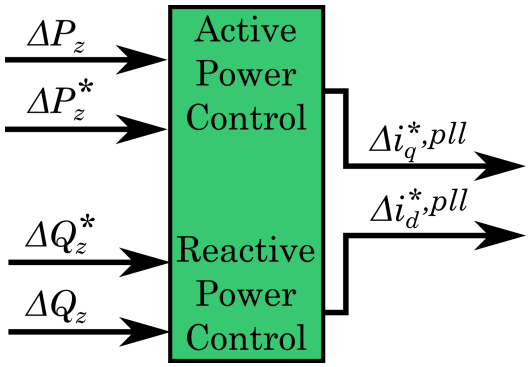

Figure 5.3: P/Q control Block

5.2.4 PPC Active and Reactive Power Control

This control subsystem consist aswell of two PI controllers that generate P and Q references to the converter's P&Q controllers to control the active and reactive power in the PCC. The input signal of the controllers is the error between the reference and measurement of P and Q in the PCC.

$e_{P_{pcc}} = P^*_{pcc} - P_{pcc}\ e_{Q_{pcc}} = Q^*_{pcc} - Q_{pcc}$

$$P^*_z = e_{P_{pcc}} \cdot (k_{p,P_{pcc}} + \int k_{i,P_{pcc}} \cdot dt) \tag{5.22}$$

$$Q^*_z = e_{Q_{pcc}} \cdot (k_{p,Q_{pcc}} + \int k_{i,Q_{pcc}} \cdot dt) \tag{5.23}$$

$$A = \begin{bmatrix} 0 & 0 \\ 0 & 0 \end{bmatrix}$$

$$B = \begin{bmatrix} 1 & 0 \\ 0 & 1 \end{bmatrix}$$

$$C = \begin{bmatrix} k_{i,P_{pcc}} & 0 \\ 0 & k_{i,Q_{pcc}} \end{bmatrix}$$

$$D = \begin{bmatrix} k_{p,P_{pcc}} & 0 \\ 0 & k_{p,Q_{pcc}} \end{bmatrix}$$

$$u = \{\Delta e_{P_{pcc}}, \Delta e_{Q_{pcc}}\}$$

$$x = \{\Delta E_{P_{pcc}}, \Delta E_{Q_{pcc}}\}$$

$$y = \{\Delta P^*_z, \Delta Q^*_z\}$$

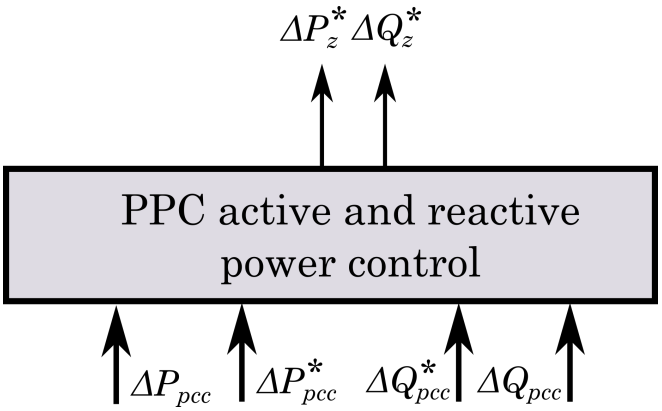

Figure 5.4: P&Q control Block at PPC

5.2.5 PLL

A PI controller is implemented in the PLL to detect the grids phase and carry out the Park transformation. An error between v^z_d and $v^{*,z}_d$ is calculated to be implemented in the State Space model. This error is filtered by the PI controller resulting in ω_{pll}.

$$e_{\omega_{pll}} = \frac{v_d^{*,z,pll} - v_d^{z,pll}}{w_b}$$

$$\omega_{pll} = e_{\omega_{pll}} \cdot (k_{p,pll} + \int k_{i,pll} \cdot dt) \tag{5.24}$$

$$A = \left[0\right]$$

$$B = \left[1\right]$$

$$C = \left[k_{i,pll}\right]$$

$$D = \left[k_{p,pll}\right]$$

$$u = \{\Delta e_{\omega_{pll}}\}$$

$$x = \{\Delta E_{\omega_{pll}}\}$$

$$y = \{\Delta \omega_{pll}\}$$

Then θ_z is obtained by integrating ω_{pll}.

$$\theta_z = \int \omega_{pll} \cdot dt \tag{5.25}$$

Its State space form is:

$$A = \left[0\right]$$

$$B = \left[1\right]$$

$$C = \left[1\right]$$

$$D = \left[0\right]$$

$$u = \{\Delta \omega_{pll}\}$$

$$x = \{\Delta W_{pll}\}$$

$$y = \{\Delta \theta_{pll}\}$$

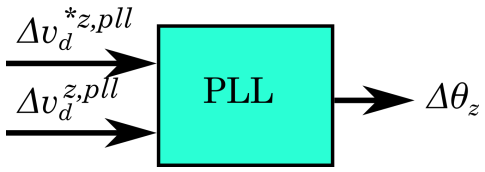

Figure 5.5: PLL Block

5.2.6 Power calculation in PCC and VSC connection point

Since the main purpose of the controllers is to manage the active and reactive power levels in different points of the system, the power needs to be calculated to be compared to the references.

Non-linear equations of power calculation in PCC:

$$P_{pcc} = \frac{3}{2} \cdot (v_q^{pcc,pll} \cdot i_q^{pll} + v_d^{pcc,pll} \cdot i_d^{pll}) \tag{5.26}$$

$$Q_{pcc} = \frac{3}{2} \cdot (v_q^{pcc,pll} \cdot i_d^{pll} - v_d^{pcc,pll} \cdot i_q^{pll}) \tag{5.27}$$

Linearized equations of power calculation in PCC:

$$P_{pcc} = \frac{3}{2} \cdot (v_q^{pcc,pll} \cdot i_{q,0}^{pll} + v_d^{pcc,pll} \cdot i_{d,0}^{pll} + v_{q,0}^{pcc,pll} \cdot i_q^{pll} + v_{d,0}^{pcc,pll} \cdot i_d^{pll}) \tag{5.28}$$

$$Q_{pcc} = \frac{3}{2} \cdot (v_q^{pcc,pll} \cdot i_{d,0}^{pll} - v_d^{pcc,pll} \cdot i_{q,0}^{pll} + v_{q,0}^{pcc,pll} \cdot i_d^{pll} - v_{d,0}^{pcc,pll} \cdot i_q^{pll}) \tag{5.29}$$

The previous equations written in state space form are:

$$A = \begin{bmatrix} 0 & 0 \\ 0 & 0 \end{bmatrix}$$

$$B = \begin{bmatrix} 0 & 0 & 0 & 0 \\ 0 & 0 & 0 & 0 \end{bmatrix}$$

$$C = \begin{bmatrix} 0 & 0 \\ 0 & 0 \end{bmatrix}$$

$$D = \begin{bmatrix} \frac{3}{2} \cdot i_{q,0}^{pll} & \frac{3}{2} \cdot i_{d,0}^{pll} & \frac{3}{2} \cdot u_{q,0}^{z,pll} & \frac{3}{2} \cdot u_{d,0}^{z,pll} \\ \frac{3}{2} \cdot i_{d,0}^{pll} & -\frac{3}{2} \cdot i_{q,0}^{pll} & -\frac{3}{2} \cdot u_{d,0}^{z,pll} & \frac{3}{2} \cdot u_{q,0}^{z,pll} \end{bmatrix}$$

$$u = \{\Delta i_q^{pll}, \Delta i_d^{pll}, \Delta u_q^{z,pll}, \Delta u_d^{z,pll}, \}$$

$$x = \{"", ""\}$$

$$y = \{\Delta P_z, \Delta Q_z\}$$

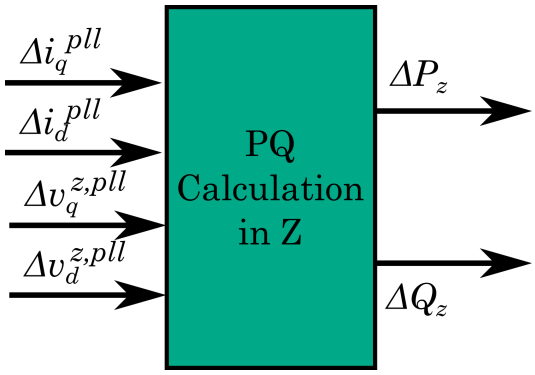

Figure 5.6: PQ calculation Block

Non-linear equations of power calculation in the VSC point of connection:

$$P_z = \frac{3}{2} \cdot (v_q^{z,pll} \cdot i_q^{pll} + v_d^{z,pll} \cdot i_d^{pll}) \tag{5.30}$$

$$Q_z = \frac{3}{2} \cdot (v_q^{z,pll} \cdot i_d^{pll} - v_d^{z,pll} \cdot i_q^{pll}) \tag{5.31}$$

Linearized equations of power calculation in the VSC point of connection:

$$P_z = \frac{3}{2} \cdot (v_q^{z,pll} \cdot i_{q,0}^{pll} + v_d^{z,pll} \cdot i_{d,0}^{pll} + v_{q,0}^{z,pll} \cdot i_q^{pll} + v_{d,0}^{z,pll} \cdot i_d^{pll}) \tag{5.32}$$

$$Q_z = \frac{3}{2} \cdot (v_q^{z,pll} \cdot i_{d,0}^{pll} - v_d^{z,pll} \cdot i_{q,0}^{pll} + v_{q,0}^{z,pll} \cdot i_d^{pll} - v_{d,0}^{z,pll} \cdot i_q^{pll}) \tag{5.33}$$

The previous equations written in state space form are:

$$A = \begin{bmatrix} 0 & 0 \\ 0 & 0 \end{bmatrix}$$

$$B = \begin{bmatrix} 0 & 0 & 0 & 0 \\ 0 & 0 & 0 & 0 \end{bmatrix}$$

$$C = \begin{bmatrix} 0 & 0 \\ 0 & 0 \end{bmatrix}$$

$$D = \begin{bmatrix} \frac{3}{2} \cdot i_{q,0}^{pll} & \frac{3}{2} \cdot i_{d,0}^{pll} & \frac{3}{2} \cdot u_{q,0}^{z,pll} & \frac{3}{2} \cdot u_{d,0}^{z,pll} \\ \frac{3}{2} \cdot i_{d,0}^{pll} & -\frac{3}{2} \cdot i_{q,0}^{pll} & -\frac{3}{2} \cdot u_{d,0}^{z,pll} & \frac{3}{2} \cdot u_{q,0}^{z,pll} \end{bmatrix}$$

$$u = \{\Delta i_q^{pll}, \Delta i_d^{pll}, \Delta u_q^{z,pll}, \Delta u_d^{z,pll}, \}$$

$$x = \{"", ""\}$$

$$y = \{\Delta P_z, \Delta Q_z\}$$

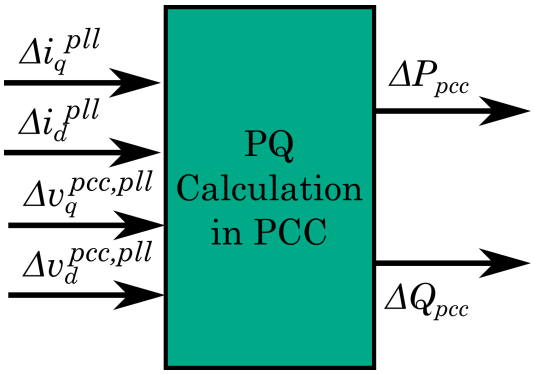

Figure 5.7: PQ at PCC calculation Block

5.2.7 Variable Frequency Generation

This subsystem can be divided in the four different state space models that together conform the model of a variable frequency power system based on thermal power plants.

$$A_1 = \begin{bmatrix} 0 & 1 \\ \frac{-1}{T_g \cdot T_{ch}} & \frac{1}{T_g + T_{ch}} \end{bmatrix}$$

$$B_1 = \begin{bmatrix} 0 \\ \frac{1}{T_g \cdot T_{ch}} \end{bmatrix}$$

$$C_1 = \begin{bmatrix} 1 & 0 \end{bmatrix}$$

$$D_1 = \begin{bmatrix} 0 \end{bmatrix}$$

$$u_1 = \{\Delta l_g\}$$

$$x_1 = \{\Delta L_g, \Delta I_g, \}$$

$$y_1 = \{\Delta p_m\}$$

$$A_2 = \begin{bmatrix} 0 \end{bmatrix}$$

$$B_2 = \begin{bmatrix} 0 & 0 \end{bmatrix}$$

$$C_2 = \begin{bmatrix} 0 \end{bmatrix}$$

$$D_2 = \begin{bmatrix} 1 & 1 \end{bmatrix}$$

$$u_2 = \{\Delta p_m, \Delta p_{LOAD}, \}$$

$$x_2 = \{"", ""\}$$

$$y_2 = \{\Delta p_{dif}\}$$

$$A_3 = \begin{bmatrix} \frac{-D}{M} \end{bmatrix}$$

$$B_3 = \begin{bmatrix} \frac{1}{M} \end{bmatrix}$$

$$C_3 = \begin{bmatrix} 1 \end{bmatrix}$$

$$D_3 = \begin{bmatrix} 0 \end{bmatrix}$$

$$u_3 = \{\Delta p_{dif}\}$$

$$x_3 = \{\Delta P_{dif}\}$$

$$y_3 = \{\Delta w\}$$

$$A_4 = \begin{bmatrix} 0 \end{bmatrix}$$

$$B_4 = \begin{bmatrix} 0 \end{bmatrix}$$

$$C_4 = \begin{bmatrix} 0 \end{bmatrix}$$

$$D_4 = \begin{bmatrix} \frac{1}{R} \end{bmatrix}$$

$$u_4 = \{\Delta w\}$$

$$x_4 = \{""\}$$

$$y_4 = \{\Delta l_g\}$$

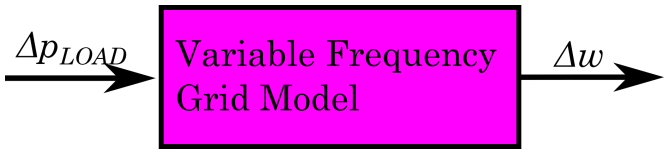

Figure 5.8: Variable Frequency Generation subsystem Block

5.2.8 Rotation Angle

In order to change from grid's reference to control reference and viceversa the angle difference between this two reference systems needs to be computed. This can be done by integrating the difference between the grid's angular speed w and w_{pll}.

$$\omega_{dif} = w - w_{pll}$$

$$\theta_{rot} = \int \omega_{dif} \cdot dt \tag{5.34}$$

$$A = \begin{bmatrix} 0 \end{bmatrix}$$

$$B = \begin{bmatrix} 1 \end{bmatrix}$$

$$C = \begin{bmatrix} 1 \end{bmatrix}$$

$$D = \begin{bmatrix} 0 \end{bmatrix}$$

$$u = \{\Delta\omega_{dif}\}$$

$$x = \{\Delta W_{dif}\}$$

$$y = \{\Delta\theta_{rot}\}$$

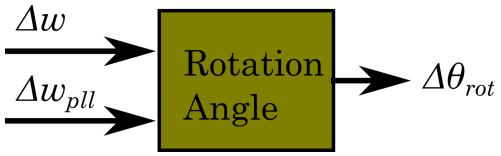

Figure 5.9: Rotation angle calculation Block

5.2.9 Reference Change

Since the connection grid equations are referenced to the grid while the controls have the PLL reference, a reference change needs to be applied to some variables. To explain this, two transformations are gonna be shown below, one from pll to grid's reference and one from grid to pll's reference.

Non-linear transformation from PLL reference to grid reference:

$$\begin{bmatrix} v_q^g \\ v_d^g \end{bmatrix} = \begin{bmatrix} cos(\theta_{rot}) & -sin(\theta_{rot}) \\ sin(\theta_{rot}) & cos(\theta_{rot}) \end{bmatrix} \begin{bmatrix} v_q^{pll} \\ v_d^{pll} \end{bmatrix}$$

Linearized transformation from PLL reference to grid reference:

$$\begin{bmatrix} v_q^g \\ v_d^g \end{bmatrix} = \begin{bmatrix} cos(\theta_{rot,0}) & -sin(\theta_{rot,0}) & -sin(\theta_{rot,0}) \cdot v_{q,0}^{pll} - cos(\theta_{rot,0}) \cdot v_{d,0}^{pll} \\ sin(\theta_{rot,0}) & cos(\theta_{rot,0}) & cos(\theta_{rot,0}) \cdot v_{q,0}^{pll} - sin(\theta_{rot,0}) \cdot v_{d,0}^{pll} \end{bmatrix} \begin{bmatrix} v_q^{pll} \\ v_d^{pll} \\ \theta_{rot} \end{bmatrix}$$

As well,the state space form of the previous linearized system is:

$$A = \begin{bmatrix} 0 & 0 \\ 0 & 0 \end{bmatrix}$$

$$B = \begin{bmatrix} 0 & 0 & 0 \\ 0 & 0 & 0 \end{bmatrix}$$

$$C = \begin{bmatrix} 0 & 0 \\ 0 & 0 \end{bmatrix}$$

$$D = \begin{bmatrix} cos(\theta_{rot,0}) & -sin(\theta_{rot,0}) & -sin(\theta_{rot,0}) \cdot v_{q,0}^{pll} - cos(\theta_{rot,0}) \cdot v_{d,0}^{pll} \\ sin(\theta_{rot,0}) & cos(\theta_{rot,0}) & cos(\theta_{rot,0}) \cdot v_{q,0}^{pll} - sin(\theta_{rot,0}) \cdot v_{d,0}^{pll} \end{bmatrix}$$

$$u = \{v_q^{pll}, v_d^{pll}, \theta_{rot}\}$$

$$x = \{"", ""\}$$

$$y = \{v_q^g, v_d^g\}$$

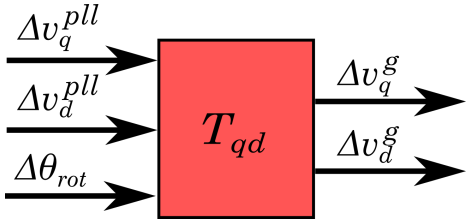

Figure 5.10: Variable Frequency block

Non-linear transformation from grid reference to PLL reference:

$$\begin{bmatrix} v_q^{pll} \\ v_d^{pll} \end{bmatrix} = \begin{bmatrix} cos(\theta_{rot}) & sin(\theta_{rot}) \\ -sin(\theta_{rot}) & cos(\theta_{rot}) \end{bmatrix} \begin{bmatrix} v_q^g \\ v_d^g \end{bmatrix}$$

Linearized transformation from PLL reference to grid reference:

$$\begin{bmatrix} v_q^{pll} \\ v_d^{pll} \end{bmatrix} = \begin{bmatrix} cos(\theta_{rot,0}) & sin(\theta_{rot,0}) & -sin(\theta_{rot,0}) \cdot v_{q,0}^g + cos(\theta_{rot,0}) \cdot v_{d,0}^g \\ -sin(\theta_{rot,0}) & cos(\theta_{rot,0}) & -cos(\theta_{rot,0}) \cdot v_{q,0}^g - sin(\theta_{rot,0}) \cdot v_{d,0}^g \end{bmatrix} \begin{bmatrix} v_q^g \\ v_d^g \\ \theta_{rot} \end{bmatrix}$$

The state space form of the previous linearized system is:

$$A = \begin{bmatrix} 0 & 0 \\ 0 & 0 \end{bmatrix}$$

$$B = \begin{bmatrix} 0 & 0 & 0 \\ 0 & 0 & 0 \end{bmatrix}$$

$$C = \begin{bmatrix} 0 & 0 \\ 0 & 0 \end{bmatrix}$$

$$D = \begin{bmatrix} cos(\theta_{rot,0}) & sin(\theta_{rot,0}) & -sin(\theta_{rot,0}) \cdot v_{q,0}^g + cos(\theta_{rot,0}) \cdot v_{d,0}^g \\ -sin(\theta_{rot,0}) & cos(\theta_{rot,0}) & -cos(\theta_{rot,0}) \cdot v_{q,0}^g - sin(\theta_{rot,0}) \cdot v_{d,0}^g \end{bmatrix}$$

$$u = \{v_q^g, v_d^g, \theta_{rot}\}$$

$$x = \{"", ""\}$$

$$y = \{v_q^{pll}, v_d^{pll}\}$$

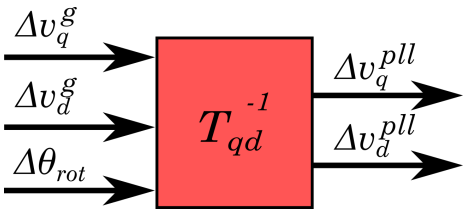

Figure 5.11: Variable Frequency block

5.2.10 Active Power reference in PCC

For the study cases in which the active power reference in the PCC, P^*_{pcc} is not fixed as a set point, it is calculated as follows.

P^*_{pcc} as a function of a frequency droop control:

$$P^*_{pcc} = K_{fdroop} \cdot \omega_{pll} \tag{5.35}$$

$$A = \begin{bmatrix} 0 \end{bmatrix}$$

$$B = \begin{bmatrix} 0 \end{bmatrix}$$

$$C = \begin{bmatrix} 0 \end{bmatrix}$$

$$D = \begin{bmatrix} K_{fdroop} \end{bmatrix}$$

$u = \{\Delta\omega_{pll}\}$ $x = \{""\}$ $y = \{\Delta P^*_{pcc}\}$

P^*_{pcc} as a function of Q^*_{pcc} and a given power factor $cos(\phi_{pcc})$ in the PCC:

$$P^*_{pcc} = \frac{Q^*_{pcc}}{tan(\phi_{pcc})} \tag{5.36}$$

$$A = \begin{bmatrix} 0 \end{bmatrix}$$

$$B = \begin{bmatrix} 0 \end{bmatrix}$$

$$C = \begin{bmatrix} 0 \end{bmatrix}$$

$$D = \left[\frac{1}{tan(\phi_{pcc})}\right]$$

$u = \{\Delta Q^{pcc}\}$ $x = \{""\}$ $y = \{\Delta P^*_{pcc}\}$

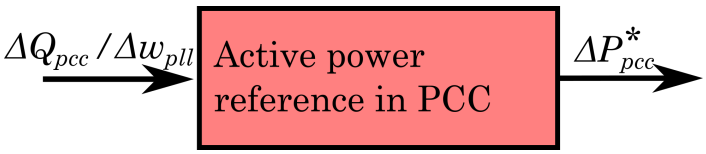

Figure 5.12: P reference at PCC Block

5.2.11 Active Power reference in PCC

The same way as with P^*_{pcc}, f the cases in which the reactive power reference in the PCC, Q^*_{pcc} is not fixed as a set point, it is calculated as follows:

Q^*_{pcc} as a function of a voltage droop control in the PCC:

$$Q^*_{pcc} = K_{vdroop} \cdot \sqrt{(v_q^{pcc,pll})^2 + (v_d^{pcc,pll})^2} \tag{5.37}$$

The linearized form of the previous equation and its state space form can be found below.

$$Q^*_{pcc} = K_{vdroop} \cdot \left(\frac{v_{q,0}^{pcc,pll} \cdot v_q^{pcc,pll}}{(v_{q,0}^{pcc,pll})^2 + (v_{d,0}^{pcc,pll})^2} + \frac{v_{d,0}^{pcc,pll} \cdot v_d^{pcc,pll}}{(v_{q,0}^{pcc,pll})^2 + (v_{d,0}^{pcc,pll})^2}\right) \tag{5.38}$$

$$A = \left[0\right]$$

$$B = \begin{bmatrix} 0 & 0 \end{bmatrix}$$

$$C = \left[0\right]$$

$$D = \left[K_{vdroop} \cdot \left(\frac{v_{q,0}^{pcc,pll}}{(v_{q,0}^{pcc,pll})^2 + (v_{d,0}^{pcc,pll})^2}\right) \quad K_{vdroop} \cdot \left(\frac{v_{d,0}^{pcc,pll}}{(v_{q,0}^{pcc,pll})^2 + (v_{d,0}^{pcc,pll})^2}\right)\right]$$

$$u = \{\Delta v_q^{pcc,pll}, \Delta v_d^{pcc,pll}\}$$

$$x = \{""\}$$

$$y = \{\Delta Q^*_{pcc}\}$$

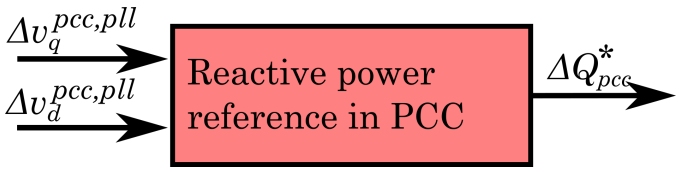

Figure 5.13: Q reference at PCC Block

Q^*_{pcc} as a function of P^*_{pcc} and a given power factor $cos(\phi_{pcc})$ in the PCC:

$$Q^*_{pcc} = tan(\phi_{pcc}) \cdot P^*_{pcc} \tag{5.39}$$

$$A = \begin{bmatrix} 0 \end{bmatrix}$$

$$B = \begin{bmatrix} 0 \end{bmatrix}$$

$$C = \begin{bmatrix} 0 \end{bmatrix}$$

$$D = \begin{bmatrix} tan(\phi_{pcc}) \end{bmatrix}$$

$u = \{\Delta P^{pcc}\}$ $x = \{""\}$ $y = \{\Delta Q^*_{pcc}\}$

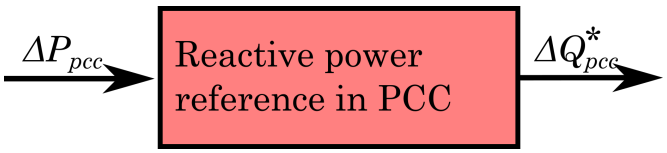

Figure 5.14: Q reference at PCC Block 3

5.2.12 Linear Model

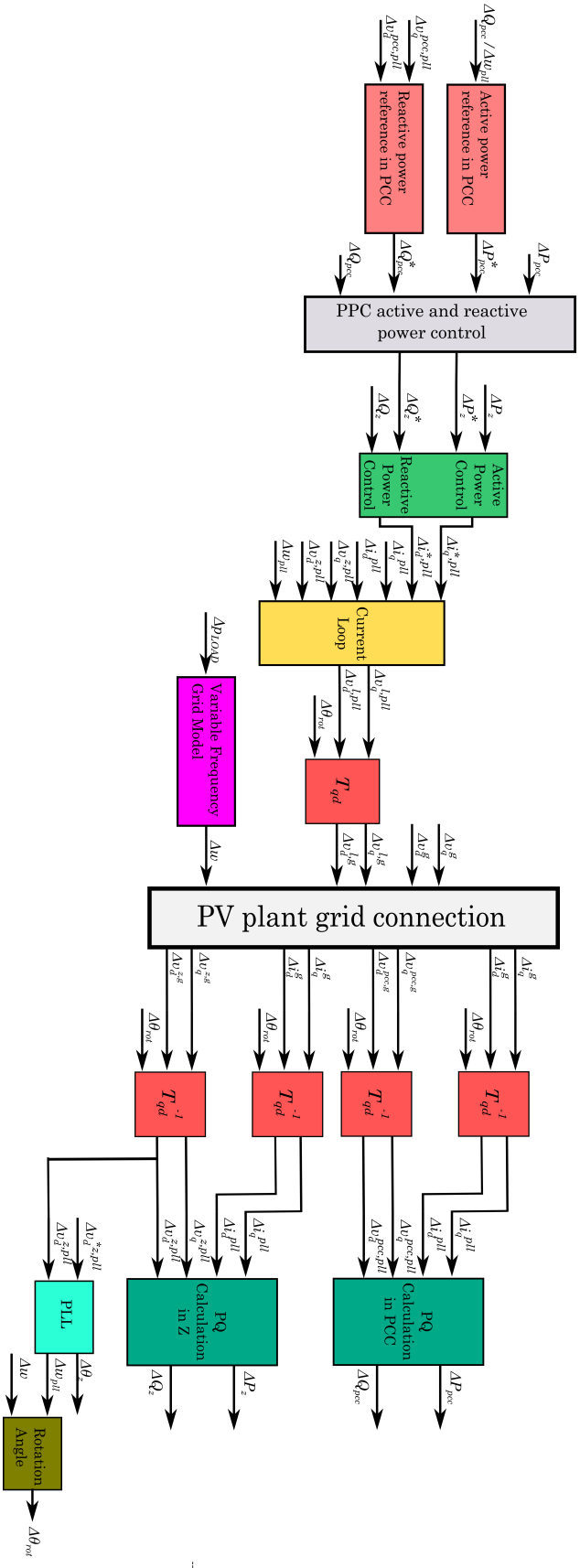

Figure 5.15: Block diagram of the linear model

5.3 Eigenvalues and Participation Factors Calculation

A way to predict how a system behaves without carrying out time domain simulations can be done by calculating its eigenvalues. In order to do achieve this goal a linear system such a State Space model is required. Then the eigenvalues can be calculated by solving the characteristic equation of the systems by applying Equation 5.40. Where A matrix comes from the State Space ,model, I is the identity matrix and λ is the eigenvalues vector.

$$det(A - \lambda \cdot I) = 0 \tag{5.40}$$

Once the eigenvalues are calculated, any positive real part eigenvalues will show unstable systems behaviour. In addition, poles with imaginary parts will also confirm the presence of second order dynamics while negative real poles are related to first order dynamics. Apart from this, information about the frequency of the oscillating mode associated to an imaginary pole the damping ratio can also be obtained:

$$f_i = \frac{Im\{\lambda_i\}}{2\pi} \tag{5.41}$$

$$\zeta = \frac{Re\{\lambda_i\}}{|\lambda_i|} \tag{5.42}$$

In addition to the eigenvalues, the contribution of different variables in a system's mode can be calculated by obtaining the system's participation factors [13]. Once a State Space model is available this task can be done easily by applying Equations 5.43 5.44 and 5.45. First the left eigenvector l_i and right eigenvector r_i are calculated. Then the participation factors can be computed. This procedure has been applied by different authors to study the impact of parameters such as SCR or cable lengths [11].

$$A \cdot r_i = \lambda \cdot r_i \tag{5.43}$$

$$l_i \cdot A = l_i \cdot \lambda \tag{5.44}$$

$$p_i^k = |r_i^k \cdot l_i^k| \tag{5.45}$$

Chapter 6

Models Validation

6.1 Introduction

The content of this chapter is related to the validation of the hypothesis undertaken during the controllers design and the small signal model developed throughout the linearization of the non-linear model.

6.2 Controllers Design

For the validation of the PPC and the converter's controller, two simulations have been carried out using the non-linear model implemented in Simulink. The objective is to check that the time response of each controller actually fulfils the time constant specifications that have been set during the design. For this purpose, step references are directly given to each of the PIs. First it is presented the results regarding the active and reactive power converter controller and the the ones from the PPC.

6.2.1 Converter Controllers

In Figure 6.1 two plots present the converter controllers response when a reactive power step and an active power step are directly given to the PIs that define the controller. The reactive power step reference given at $t = 0$ is Q_z^* =0.33 while the active power reference is P_z^* =0.95. First of all it can be seen that both curves match first order dynamics. Then,

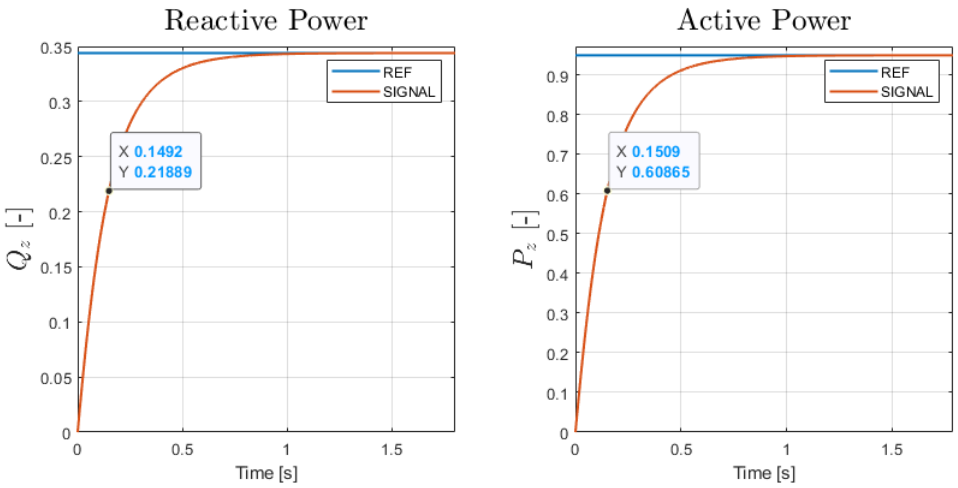

Figure 6.1: Converter Reactive and Active power response

regarding the curves time constant, it must be verified that for the time instant equal to the time constant $t = \tau_z$ =0.15 s, both responses achieve a very close value to the $\%63$ of their respective input references. These values are respectively $Q_z^*(\tau_z) = 0.21$ and $P_z^*(\tau_z) = 0.59$. This way it can be validated the hypothesis considered are good enough for the converter controllers design.

6.2.2 PPC

The same simulation has been carried out again considering the PI controllers from the PPC. In Figure 6.2 the active power and reactive power response in the PCC are plotted when two step references are given in $t = 0$.

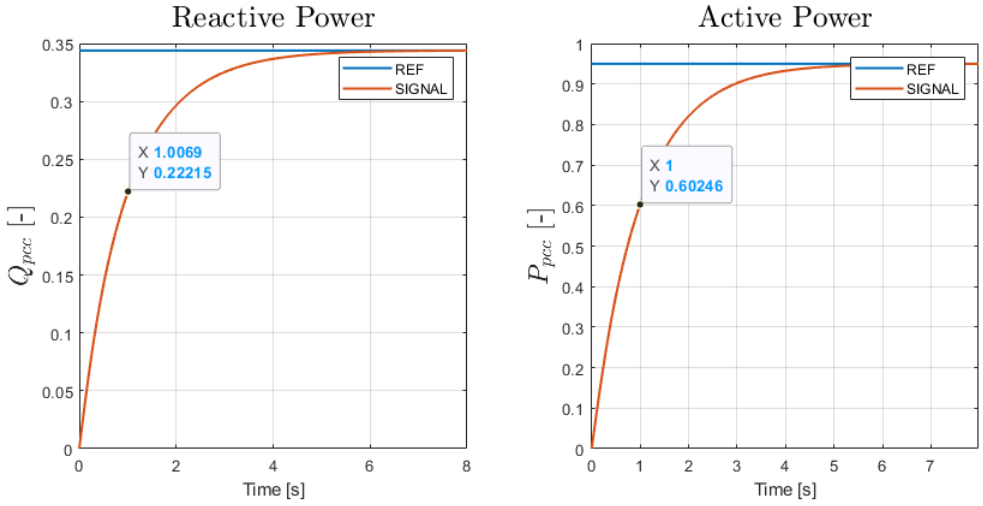

Figure 6.2: PPC response

As expected the two signals follow first order dynamics. As well, they fulfill time constant specifications since in t= τ_{pcc} =1 s each signal meets a very close value to the one they are supposed to reach:$Q_z^*(\tau_z) = 0.21$ and $P_z^*(\tau_z) = 0.59$.

6.3 Linear Model

This part of the thesis presents the validation of the previously explained linear model . This procedure basically consists on comparing the response from the two models, the linear and the non-linear. In case the linearized model tracks the non-linear model simulation, the linearized model can be validated. To do so, it is important that the two models are run considering the same boundary conditions: same operating points and synchronized reference changes.

Another important point to be considered during this process is related to the potential unavoidable deviation that can be found between the two models outcomes. The reason why this might happen is that the linearized model is an approximation obtained from the non-linear model at a certain operation point as explained before. This way the more is the change in the operating conditions, the less accurate can be the linear response since the new operating conditions are far different from the ones used to linearize the system. To visualize this, the same variable are plotted for two cases, the first one considering a $\%5$ step increase in the active power in the PCC and the second one considering a $\%30$ increase. As it can be seen in Figures 6.4 and 6.3, when the step is not small (5% or less), the response of the linear and non-linear models can differ a lot and therefore the model is no longer representative and useful. Due to this issue the different scenarios considered for the study will be validated applying a 1% reference change.

6.3.1 Case 1 : PQ setpoint

The outcome from the linear model with direct reference setpoints control can be seen in the following figures. In each plot the response of the linear(blue) and non-linear(orange) models are put together. For all plots the linear model results always starts from an equilibrium point that has been used to linearize the model. When looking at the non-linear results, they all have an initial transient. After the non-linear reaches steady state, an active power

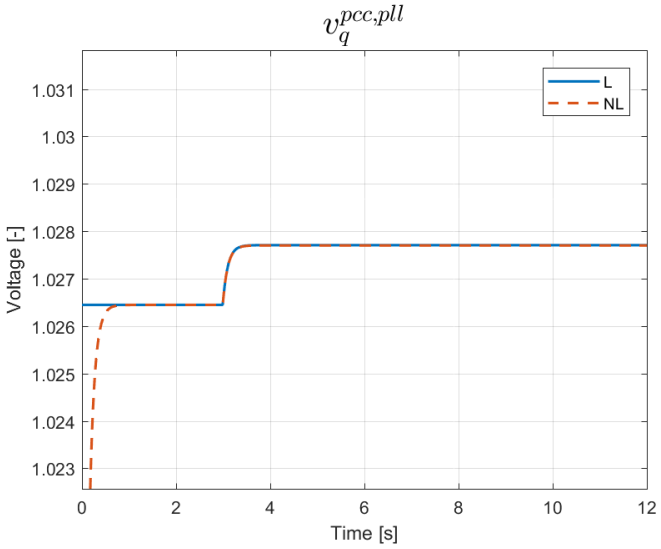

Figure 6.3: $v_q^{pcc,pll}$ after a 5% increase in P_{pcc}^*

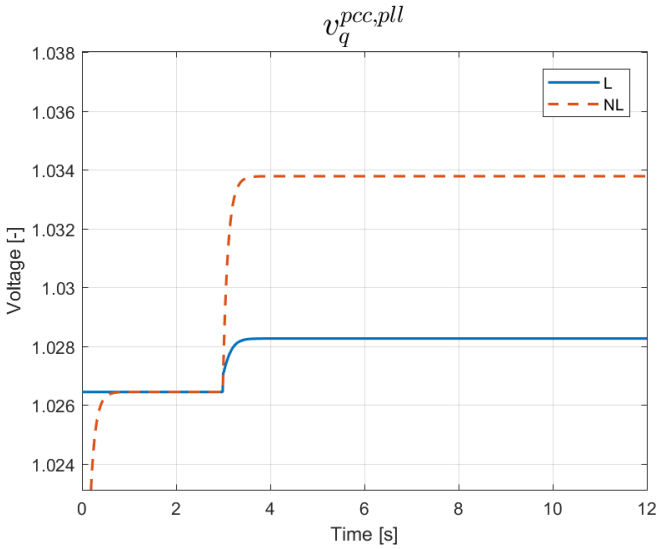

Figure 6.4: $v_q^{pcc,pll}$ after a 30% increase in P_{pcc}^*

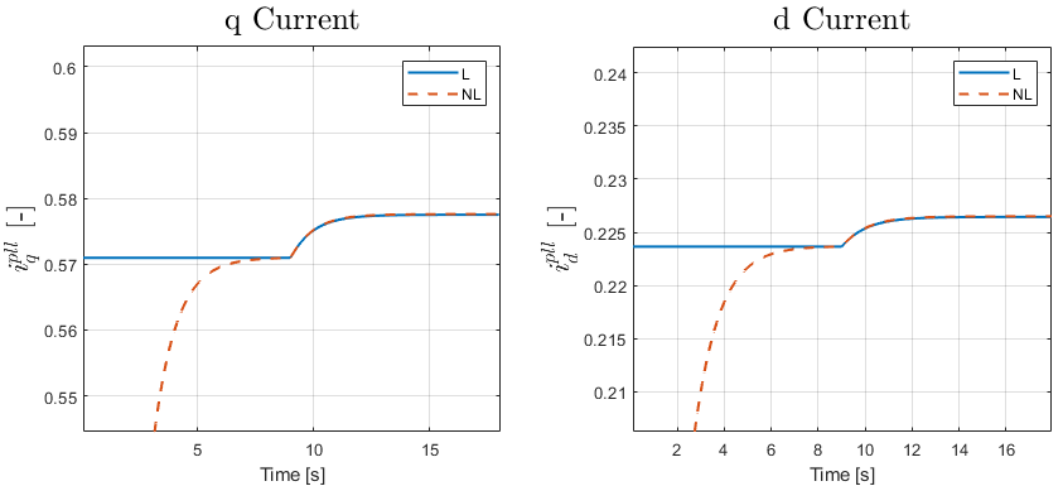

Figure 6.6: Comparison of current responses. Case 1

reference step of $\%1$ is applied. In Figures 6.5 6.6 6.7 it can be seen that the new transient takes place at t =9 s.

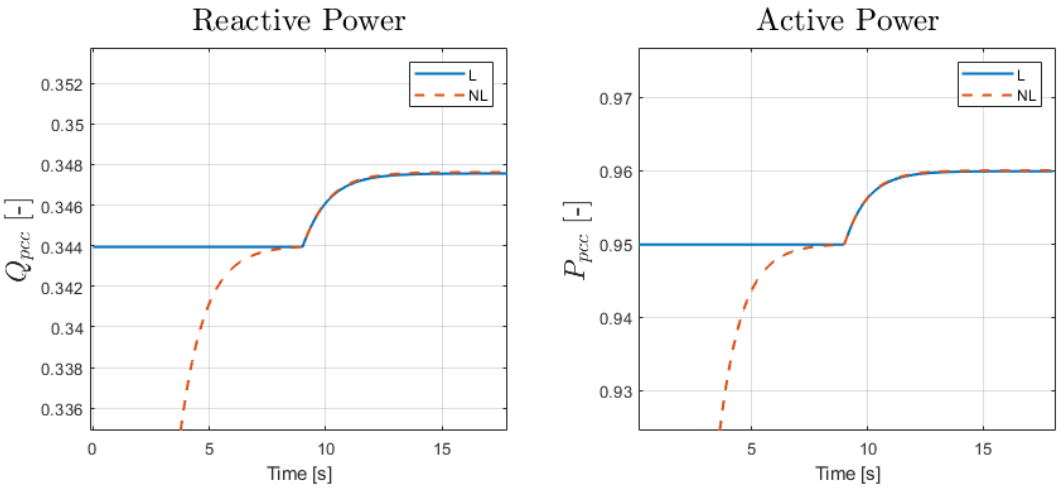

Figure 6.5: Comparison of Power Responses. Case 1.

In Figure 6.5 the power responses for both active and reactive magnitudes can be seen. As it can be appreciated the dynamics followed by the two models are exactly the same, achieving eventually equal steady values. The q and d components of the current that is injected into the grid can be seen in Figure 6.6. Similar results are obtained in this case, matching transient and final steady values. The voltage in the point of common coupling is also compared in Figure 6.7. There it can be seen how there is a slight deviation between the two models response in the q component of the voltage. However the dynamics match perfectly so that the model can be validated.

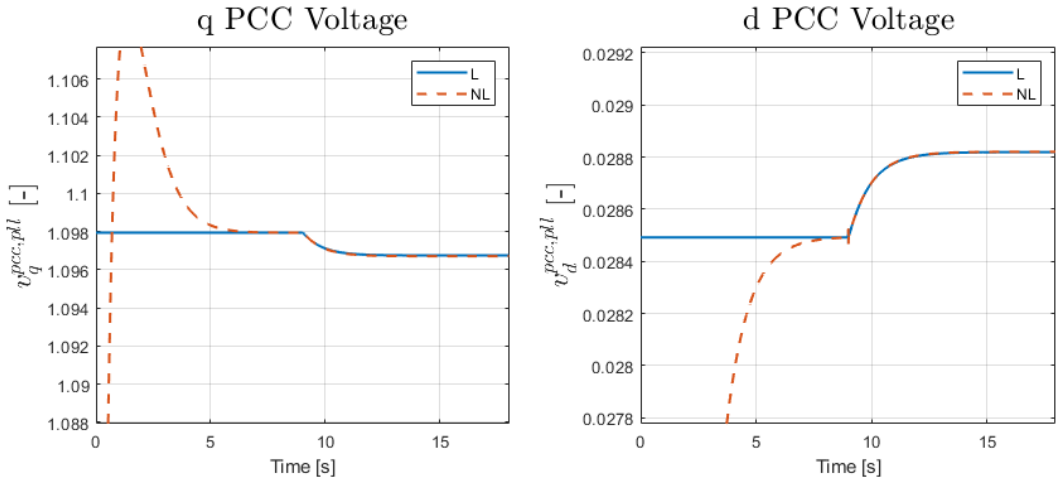

Figure 6.7: Comparison of voltage responses in PCC. Case 1

6.3.2 Case 2 : Voltage Droop Control

In this part it is validated the linear model with voltage droop control. This model has been simulated by applying a $\%1$ reduction in the ideal three phase voltage sources used in the Thevenin equivalent of the grid. Regarding the linear model, this is directly translated into a grid voltage step. After the non-linear reaches steady state, a frequency change is applied on the system. The transient produced in t =6 s for the different variables considered can be seen in Figures 6.8, 6.9, 6.10.

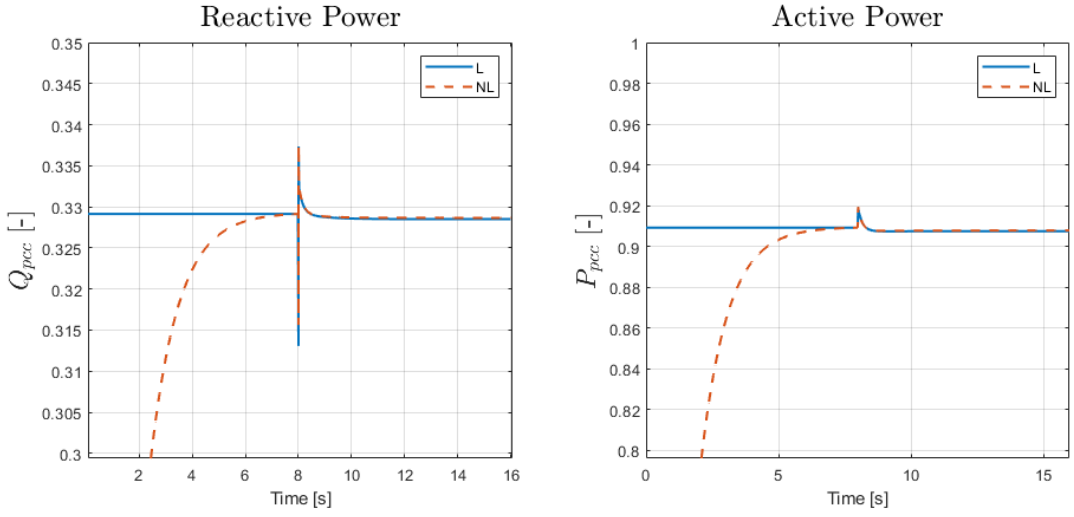

Figure 6.8: Comparison of power responses. Case 2

The power responses for both active and reactive magnitudes is presented in Figure 6.5. There it can checked that both linear variables follow the non-linear response during the whole transient till the final value. As well it can be pointed out that the power references

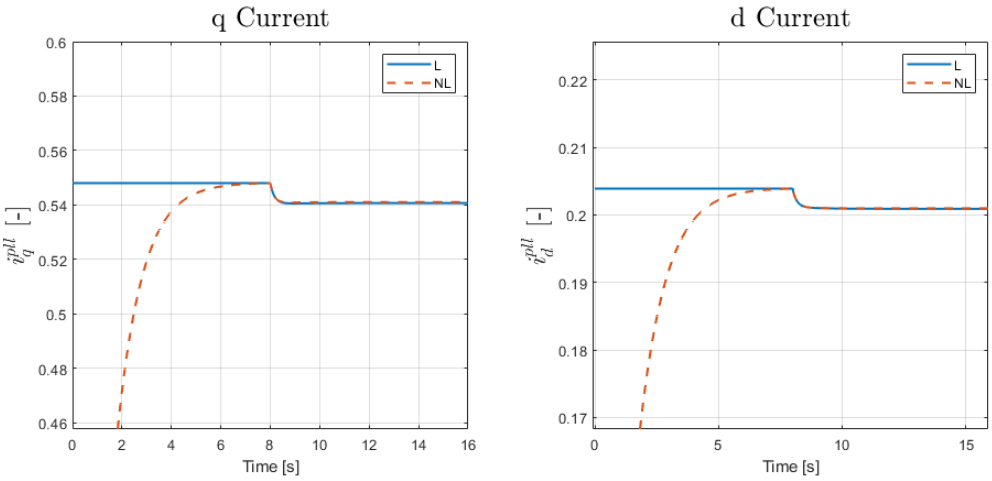

Figure 6.9: Comparison ff current responses. Case 2

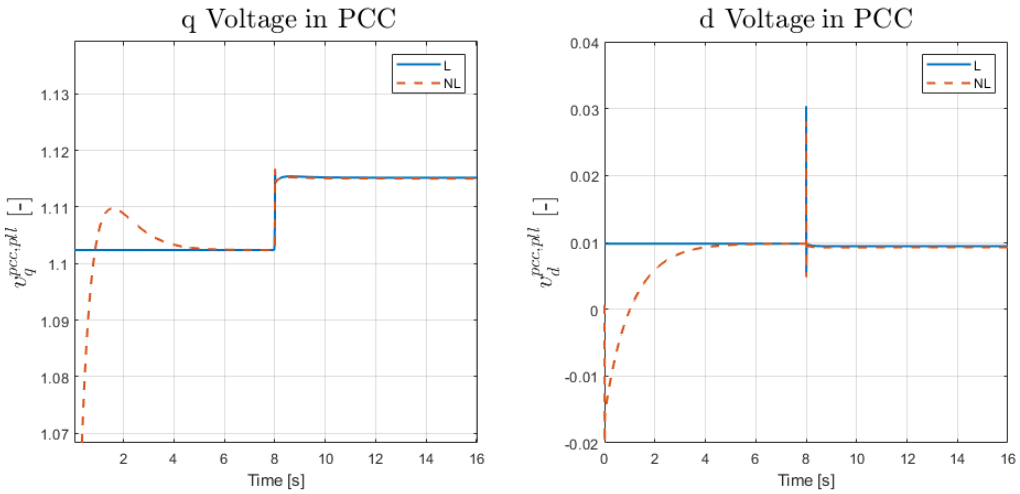

Figure 6.10: Comparison of voltage responses in PCC. Case 2

are reduced due to the frequency increase and the negative slope of the frequency droop. The q and d components of the current that is injected into the grid can be seen in Figure 6.9. Similar results are obtained in this case, matching transient and final steady values. The voltage in the point of common coupling is also compared in Figure 6.10. Again for both cases the linear model resembles up to great extent the non-linear responses. This way this model is also validated.

6.3.3 Case 3 : Frequency Droop Control

In this section the results from the frequency droop linear model are presented along the non-linear results. In second t=10 s a load reference change is generated in the frequency response model, propagating a second order oscillation to the rest of the system magnitudes

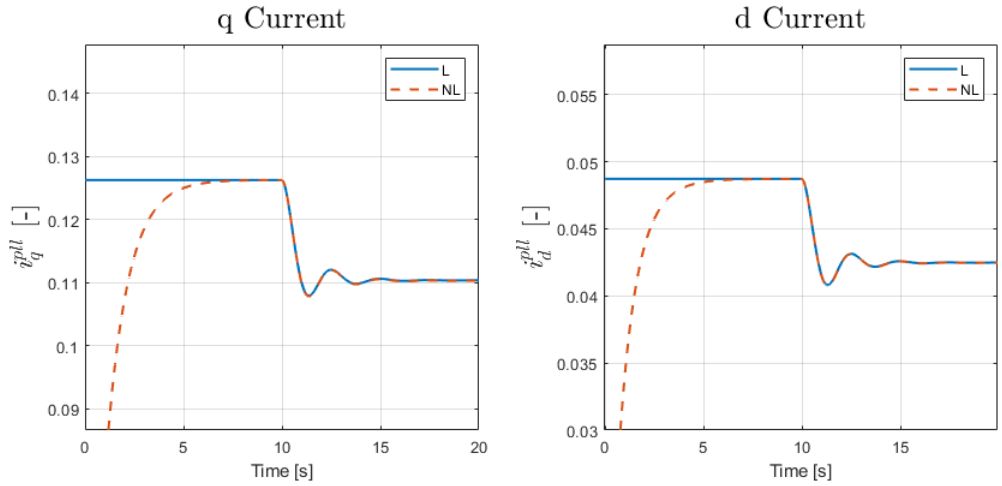

Figure 6.12: Comparison pf current responses. Case 3

through the power active reference of the PPC. The main signals responses can be seen in Figures 6.11 6.12 6.13.

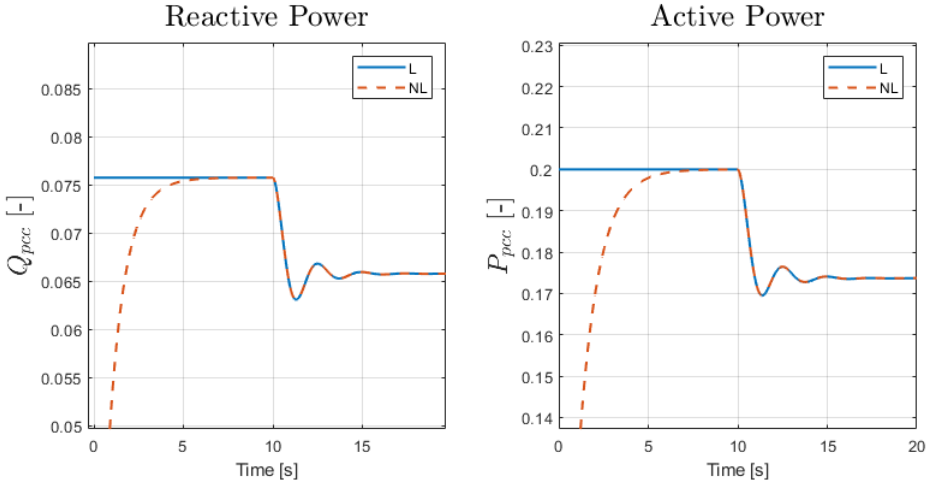

Figure 6.11: Comparison of power responses. Case 3

The power responses for both active and reactive magnitudes can be seen in Figure 6.11.Comparing the two model responses it can be seen that they are basically equal. Both current component magnitudes can also be found for this case in Figure 6.12, where it can be verified that the linear model tracks the non-linear one, being the d component more accurate. Finally the voltage in the point of common coupling is also compared in Figure 6.13, where a little deviation between the two models responses can be appreciated. Nevertheless, the dynamics are properly traced and the deviation is really small considering the total signal variation between steady states. Thus the model is validated.

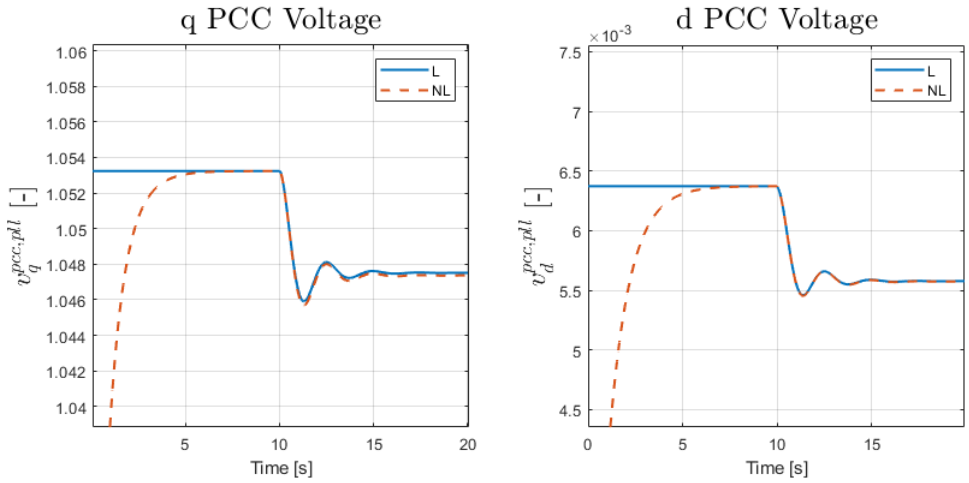

Figure 6.13: Comparison of voltage responses in PCC. Case 3

Chapter 7

Dynamics Analysis

7.1 Introduction

The following chapter summarizes the results obtained from a series of simulations carried out considering the different case scenarios presented previously. As a part of this process, pole diagrams, participation factors and time domain simulations are shown to try to figure out the dynamic trends of the system when speeding up the Power Plant Controller. With the aim of comparing each of these scenarios, the same set of PPC time constants have been used in every case. These values can be found in in Table 7.2.3.

Value	τ_{pcc} (s)
1	1
2	0.72
3	0.44
4	0.15

Table 7.1: Different time constant values considered

7.2 Case 1: PQ reference setpoints

7.2.1 Eigenvalues locus

Due to the PPC time constant reduction, the dynamics of the system are affected up to a certain point. These characteristics are directly linked to the the eigenvalues of the linear model A matrix, which have been calculated and are presented in Figure 7.1 . Such plot has been built by using 4 different values of PPC time constant gathered in Table 7.2.3 plus a fifth one τ_{pcc}=0.1s.

When it comes to the pole location, both real poles and conjugated imaginary poles can be found, remarking that there is just a pair of conjugated poles for each value of time constant. Besides, no poles with positive real part have been found, what guarantees system's stability for the different time constants considered.

7.2.2 Participation Factor Analysis

As a part of the dynamics analysis, participation factors have been calculated for the different time constant considered. However, only the results regarding the first value are presented in this section due to the similarity in the results from the different time constant values. The participation factors regarding the first case are gathered in Figure 7.2. The different Modes can be found along their frequencies and damping ratios can be found in the first three rows. On the left, the states variables are ordered in a column, being the inner table values the participation of each state variable on each Mode. Regarding the participation magnitudes, they are scaled so that the no involvement is quantified with a 0 and the maximum from all the participators with a value of 1. The different modes are explained as follows:

- Mode 1 and 2 correspond to a pair of conjugated poles that can be linked to the PLL performance, since the greater participating factors are related to the angular speed calculation and input error of the PLL's PI. As well, it can be highlighted the participation of the state related to the d current component.

- Modes 3 and 4 are two conjugated poles with very low frequency. These two modes relate the current two current components with the angular speed state from the PLL.

- Modes 5, 6, 7 and 8 are four non-osicllating modes in which the the main participating

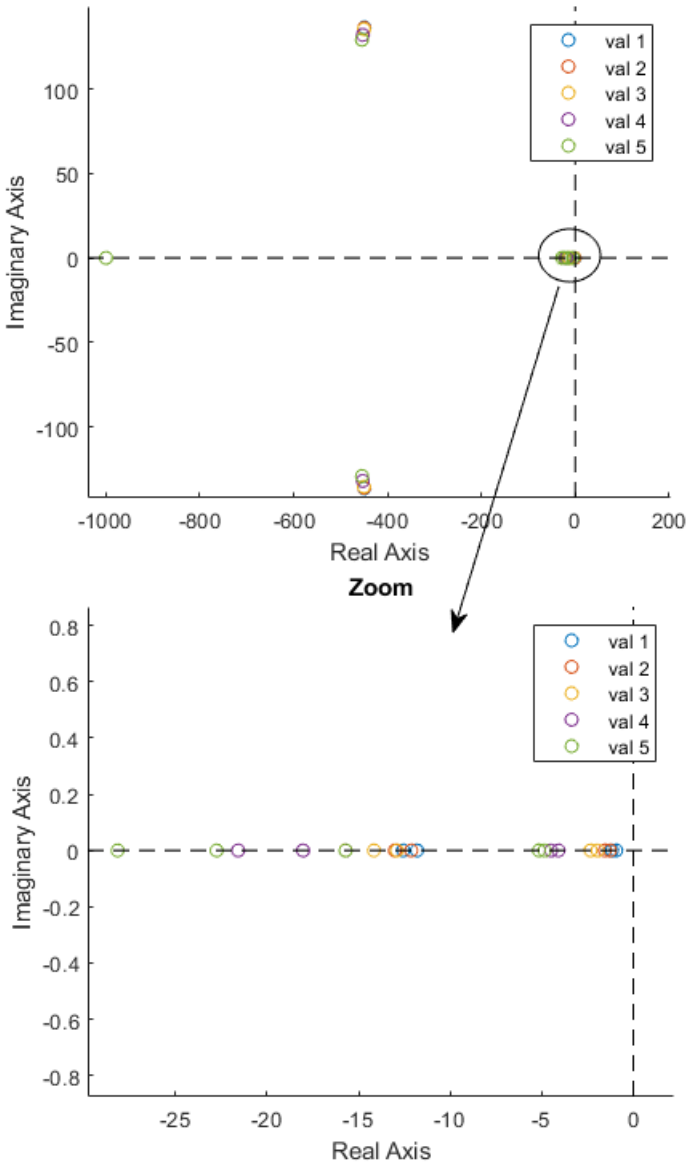

Figure 7.1: Pole Diagram. Case 1

Val. 1	Mode 1	Mode2	Mode3	Mode4	Mode5	Mode6	Mode7	Mode8	Mode9	Mode10
f (Hz)	21,72	21,72	0,00	0,00	0,00	0,00	0,00	0,00	0,00	0,00
damp	0,96	0,96	1,00	1,00	1,00	1,00	1,00	1,00	1,00	1,00
I_q	0,03	0,03	0,52	0,52	0,00	0,00	0,03	0,01	0,07	0,07
I_d	0,28	0,28	1,00	1,00	0,00	0,00	0,01	0,03	0,08	0,08
ErP_z	0,00	0,00	0,00	0,00	0,08	0,00	1,00	0,12	0,00	0,00
ErQ_z	0,01	0,01	0,02	0,02	0,00	0,09	0,12	1,00	0,00	0,00
ErPpcc	0,00	0,00	0,00	0,00	1,00	0,00	0,08	0,01	0,00	0,00
ErQpcc	0,00	0,00	0,00	0,00	0,00	1,00	0,01	0,09	0,00	0,00
ErIq	0,00	0,00	0,01	0,01	0,00	0,00	0,05	0,01	0,98	0,98
ErId	0,00	0,00	0,01	0,01	0,00	0,00	0,01	0,06	1,00	1,00
ErPLL	0,79	0,79	0,00	0,00	0,00	0,00	0,00	0,00	0,00	0,00
W	1,00	1,00	0,49	0,49	0,00	0,00	0,01	0,01	0,01	0,01

Figure 7.2: Participation Factors. Case 1

state variables are the input error of the active PI PCC controller, reactive PI PCC controller,active PI converter controller and reactive PI converter controller respectively. About Modes 7 and 8 it can be appreciated a small interaction between the two input errors of the power converter controller.

- Modes 9 and 10 can be involved with a conjugated pair of poles related to the current controller. There it can be seen how the input errors of the current controller participate the most.

7.2.3 Time domain simulations

The system's time domain response under these conditions can be seen in Figure 7.3, 7.4, 7.5, 7.6, where the converters voltage, PCC voltage, current and powers are plotted respectively for the different τ_{pcc} defined in table ref. Regarding all these plots, one of the main features to highlight is how despite the PPC's speed-up , first order dynamics are kept for all the variables but for the d components of the converter and PPC voltages. As well, it can be confirmed that in every case the lower is τ_{pcc}, the faster is achieved the next steady state.

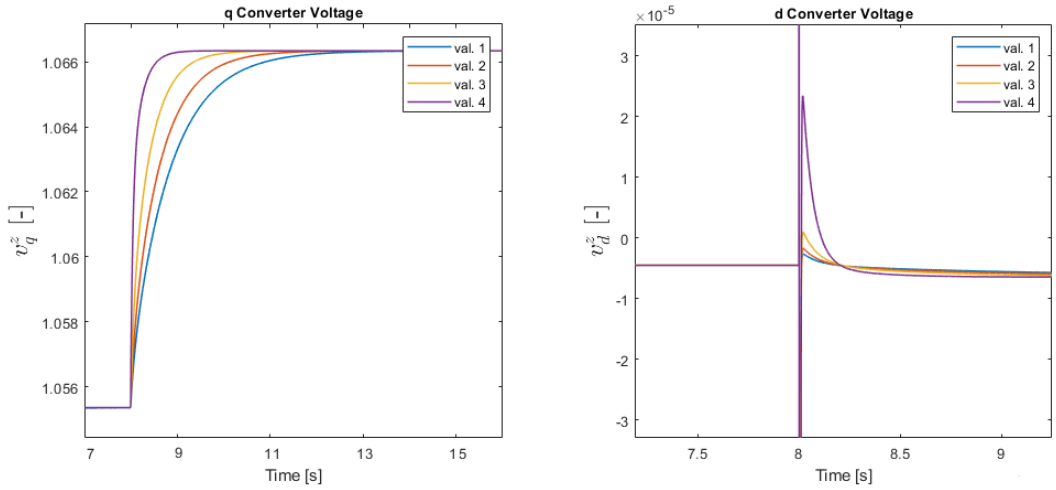

Figure 7.3: Comparison of converter's voltage response. Case 1

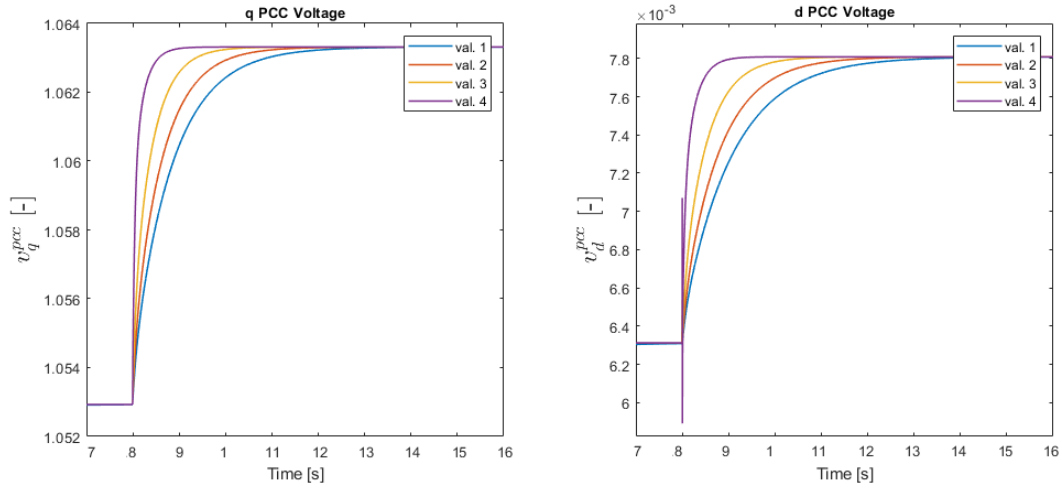

Figure 7.4: Comparison of voltage responses in PCC. Case 1

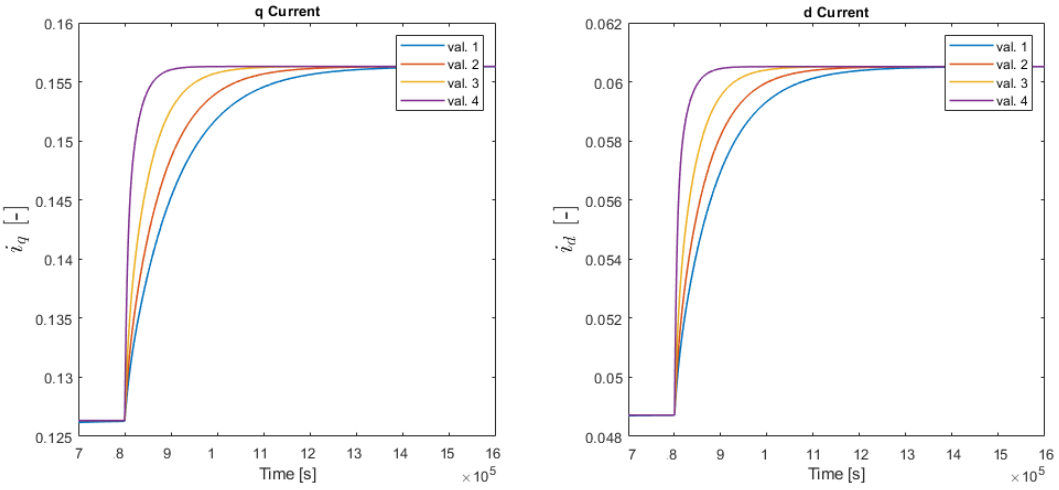

Figure 7.5: Comparison of current responses. Case 1

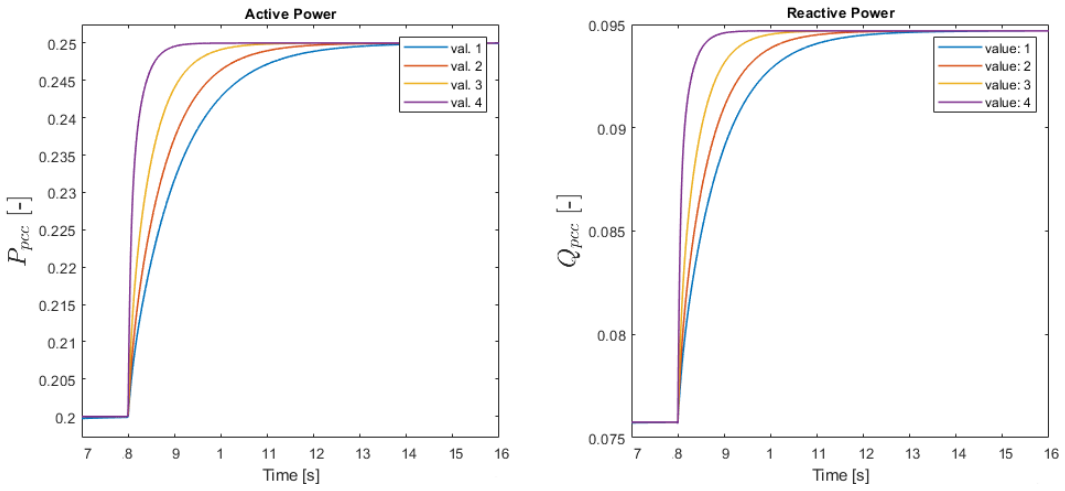

Figure 7.6: Comparison of power responses. Case 1

7.3 Case 2: Voltage droop

7.3.1 Eigenvalues Locus

The system's poles calculation has been carried out for the Voltage droop control mode considering the same time constants used in the previous case. Regarding the results presented in Figure 7.7 from this analysis, first of all it can be seen that there are no unstable poles. On the other hand, it can also be pointed out that for every case calculated, the poles location are very similar in far regions from the origin. There, every time constant value sets a pair of conjugated poles around -200 in the real axis. When zooming in closer to the origin the majority of the poles are found. In this region a pair of conjugated poles of very low frequency are placed for every case as well an additional pair conjugated poles for the fourth and fifth values.

7.3.2 Participation Factors

In Figure 7.8 the different Modes and participating factors obtained for this case can be seen. The most relevant information extracted from such results can be read as follows:

- Mode 1 and 2 correspond to the low frequency oscillations that take place on the currents.
- Mode 3 and 4 are related to the PLL performance, since the input error and the angular frequency calculation are the mainly states involved.

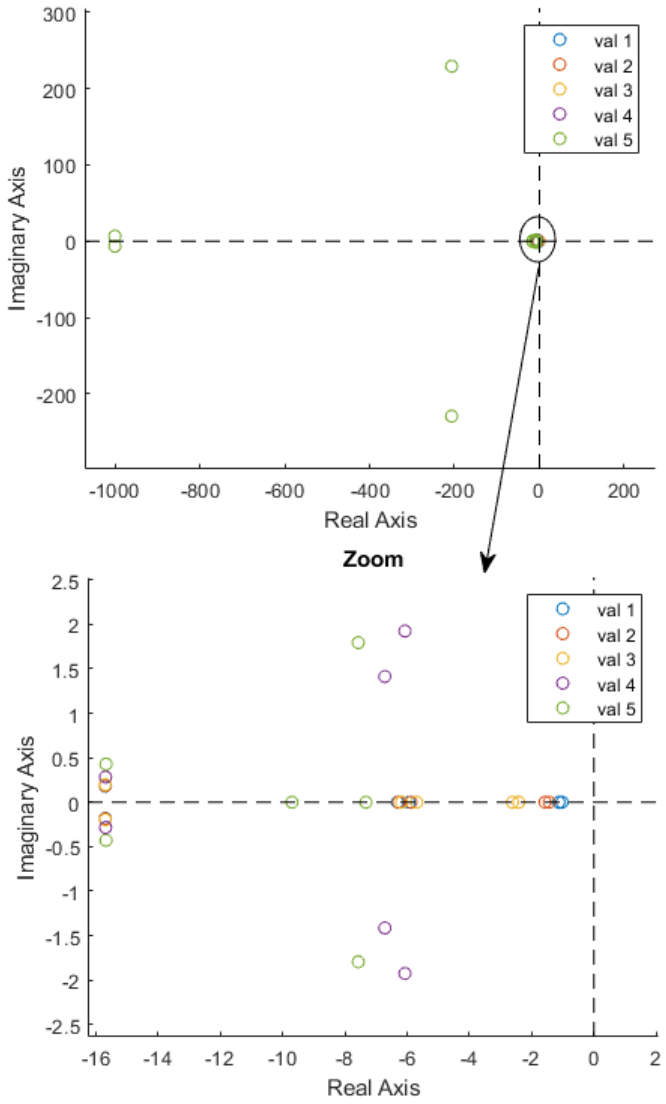

Figure 7.7: Poles Diagram. Case 2

Val. 1	Mode1	Mode2	Mode3	Mode4	Mode5	Mode6	Mode7	Mode8	Mode9	Mode10
f (Hz)	1,05	1,05	36,49	36,49	0,03	0,03	0,00	0,00	0,00	0,00
damp	1,00	1,00	0,67	0,67	1,00	1,00	1,00	1,00	1,00	1,00
I_q	0,92	0,92	0,01	0,01	0,03	0,03	0,00	0,00	0,00	0,00
I_d	1,00	1,00	0,06	0,06	0,03	0,03	0,00	0,00	0,00	0,00
ErP_z	0,01	0,01	0,00	0,00	0,01	0,01	0,55	1,00	0,17	0,01
ErQ_z	0,01	0,01	0,00	0,00	0,01	0,01	1,00	0,57	0,01	0,18
ErPpcc	0,00	0,00	0,00	0,00	0,00	0,00	0,10	0,16	1,00	0,06
ErQpcc	0,00	0,00	0,00	0,00	0,00	0,00	0,18	0,11	0,05	1,00
Erlq	0,01	0,01	0,00	0,00	1,00	1,00	0,00	0,01	0,00	0,00
Erld	0,01	0,01	0,00	0,00	1,00	1,00	0,02	0,00	0,00	0,00
ErPLL	0,00	0,00	0,98	0,98	0,00	0,00	0,00	0,00	0,00	0,00
W	0,08	0,08	1,00	1,00	0,00	0,00	0,00	0,00	0,00	0,00

Figure 7.8: Partification Factors. Case 2

- Mode 5 and 6 are slightly oscillating modes associated with the input errors of the current loop.

- Mode 7, 8 are non-oscillating modes. The variables related to this nodes are input erros from the PPC PIs and the Active and Reactive controllers of the converter's controller. About these modes, it is remarkable how the error signals from the active and reactive PI controllers interact despite the non-obvious link.

- Mode 9 and 10 are non-oscillating modes which relate the states of the PI controllers that deal with Active and Reactive power in the PPC and the converter's controller independently.

7.3.3 Time domain simulations

Time domain simulations have been carried out for the voltage droop control mode considering thefour time constant values from Table 7.2.3. These simulations have been developed by applying a decrease step in the voltage amplitude of the ideal voltage sources considered on the AC grid. As a result an abrupt transient can be seen in Figures 7.9, 7.10, 7.11, 7.12, where the the converter voltage, the PCC voltage, the current and the powers are represented respectively. From these plots it can also be seen most of the signals obtained follow first order dynamics. It is just for the fourth value of time constant which generates a small overshoot in the current and power magnitudes. To conclude, a small second order oscillation can also be seen in the d component of the converter's voltage.

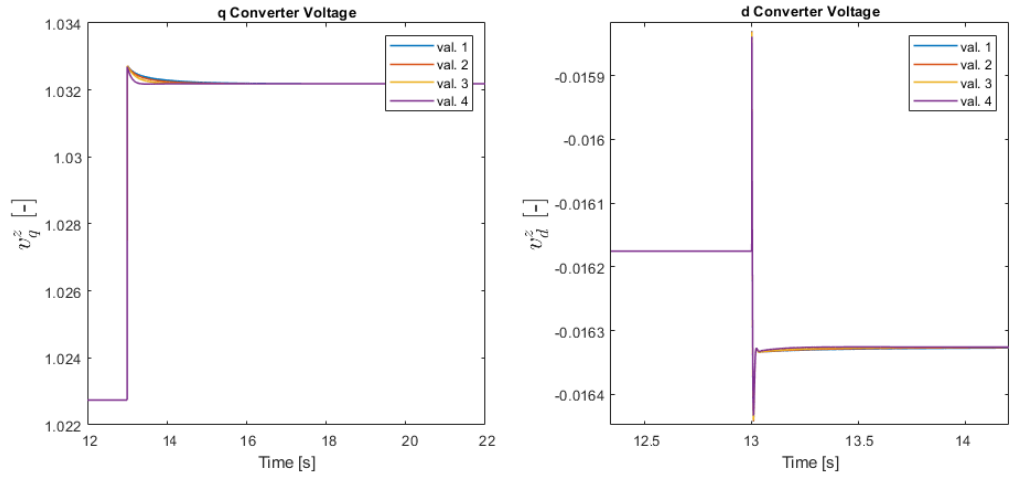

Figure 7.9: Comparison of converter's voltage responses. Case 2

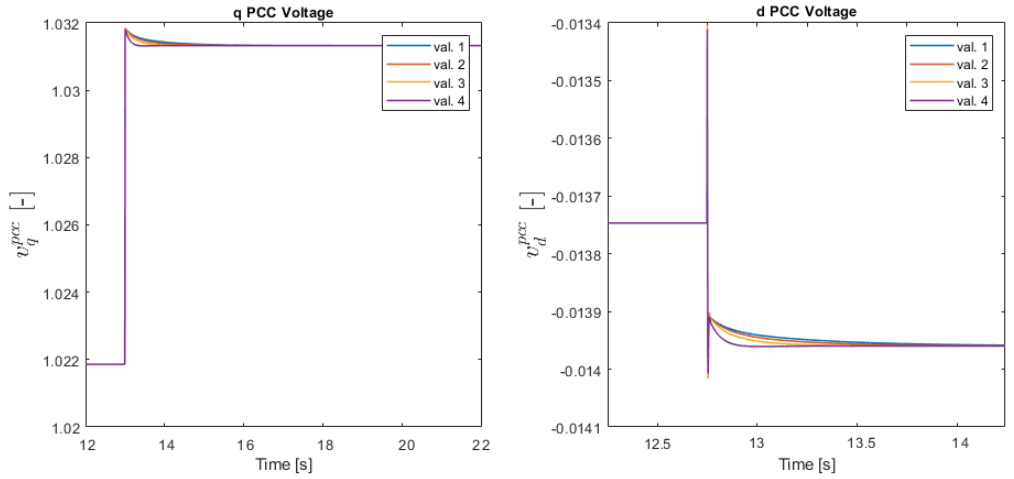

Figure 7.10: Comparison of PCC voltage responses. Case 2

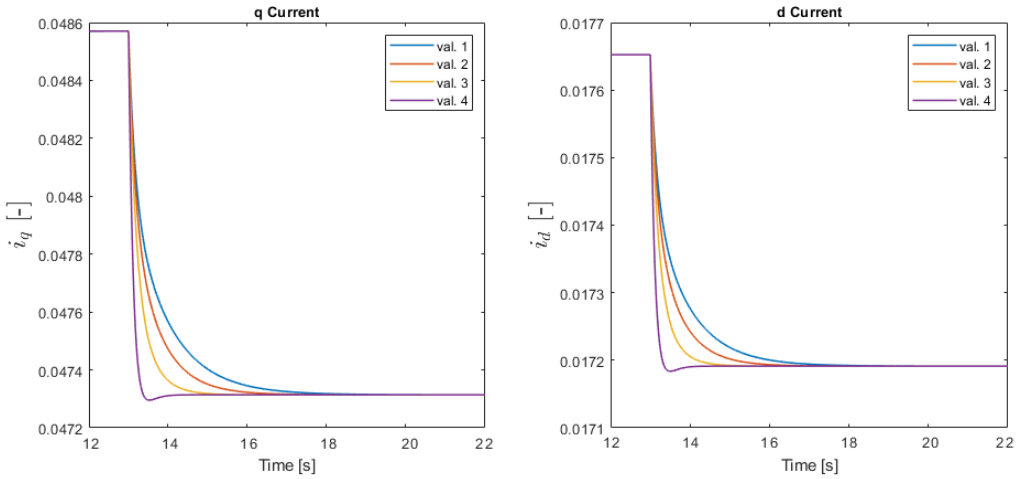

Figure 7.11: Comparison of current responses. Case 2

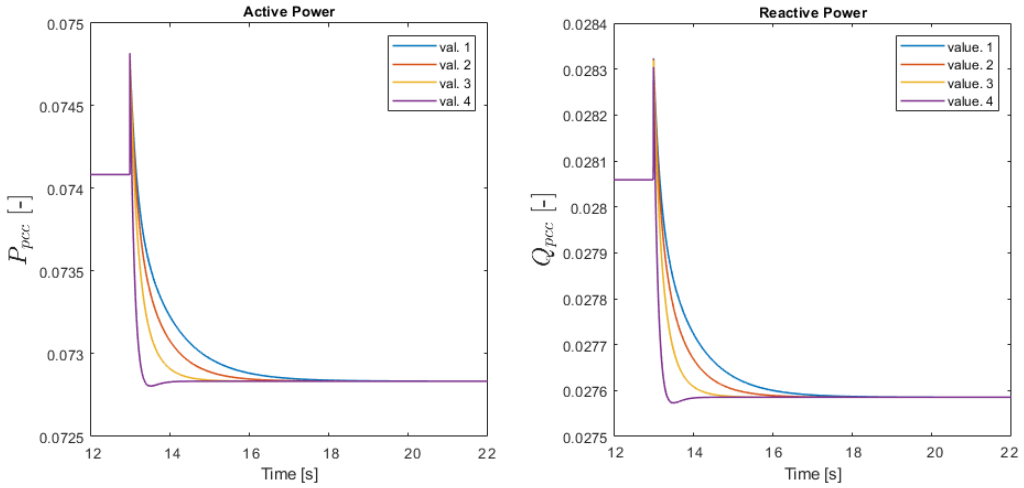

Figure 7.12: Comparison of powers responses. Case 3

7.4 Case 3. Frequency droop

7.4.1 Eigenvalues Locus

The poles that have been found in this case are plotted in Figure 7.13 for the same five time constants used previously. It can be appreciated how there are two pairs of poles that are replicated in the same say for every time constant value, one close to the origin and another one far from it. As well it can be seen how for the fourth and fifth value of time constant two more pairs of poles can be seen in the zoomed-in plot. Similarly one more pair of imaginary poles appears close to them.

7.4.2 Participation Factors

Participation factors have been calculated for every value of time constant considered. In this case two different tables with the first and fourth value of time constant are presented in Figure 7.15 and 7.14 accordingly. There it can be seen how there are several differences such as number of oscillating modes and the frequency of the common oscillating modes. Regarding the first scenario modes:

- Modes 1 and 2 represent a pair of conjugated poles where the PLL states have a great influence. As well it seems interesting the relatively high participation of the current states in this mode.

- Modes 3 and 4 can be associated to two conjugated imaginary poles with tiny fre-

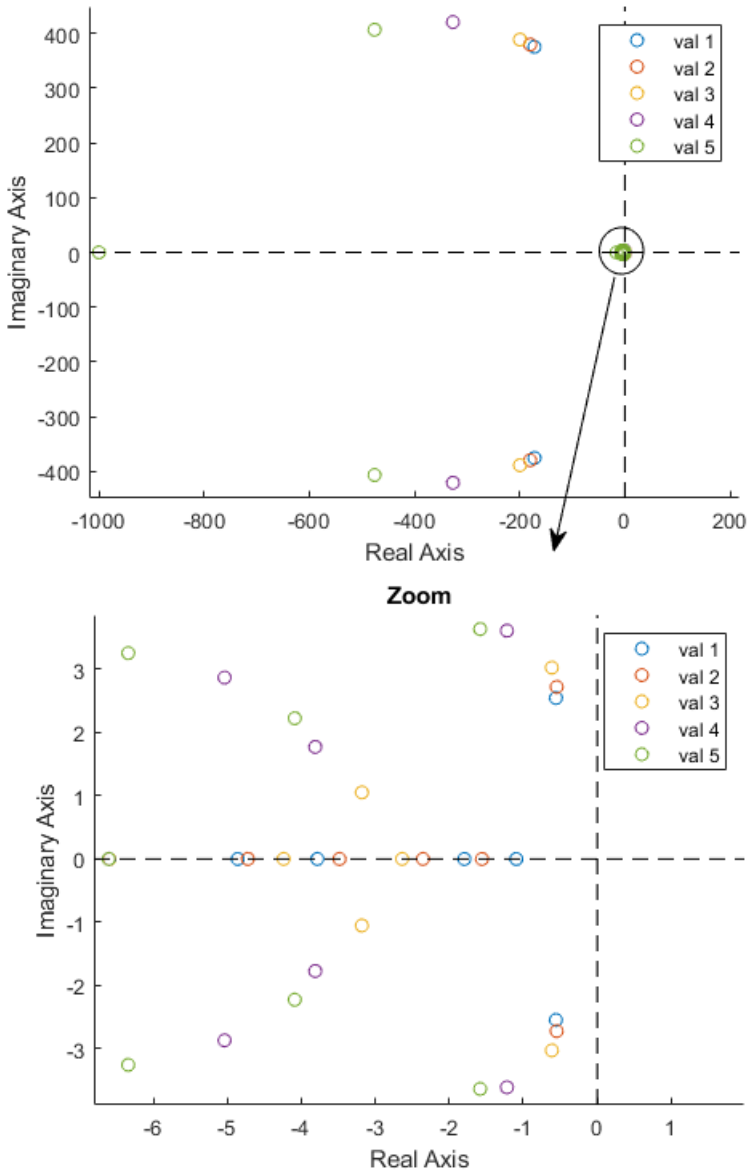

Figure 7.13: Pole Diagram. Case 3

Val. 4	Mode1	Mode2	Mode3	Mode4	Mode5	Mode6	Mode7	Mode8	Mode9	Mode10	Mode11	Mode12	Mode13
f (Hz)	66,88	66,88	0,00	0,00	0,58	0,58	0,00	0,28	0,28	0,46	0,46	0,00	0,00
damp	0,61	0,61	1,00	1,00	0,32	0,32	1,00	0,91	0,91	0,87	0,87	1,00	1,00
FreqR1	0,00	0,00	0,00	0,00	0,55	0,55	0,26	0,54	0,54	0,01	0,01	0,00	0,00
FreqR2	0,00	0,00	0,00	0,00	0,27	0,27	1,00	0,47	0,47	0,01	0,01	0,00	0,00
FreqR3	0,00	0,00	0,00	0,00	1,00	1,00	0,12	0,05	0,05	0,01	0,01	0,00	0,00
Iq	0,59	0,59	1,00	1,00	0,00	0,00	0,00	0,01	0,01	0,00	0,00	0,02	0,02
Id	0,48	0,48	0,85	0,85	0,00	0,00	0,00	0,00	0,00	0,00	0,00	0,03	0,03
ErPz	0,21	0,21	0,18	0,18	0,41	0,41	0,00	1,00	1,00	0,43	0,43	0,00	0,00
ErQz	0,16	0,16	0,19	0,19	0,07	0,07	0,01	0,49	0,49	1,00	1,00	0,00	0,00
ErPpcc	0,00	0,00	0,00	0,00	0,51	0,51	0,01	0,88	0,88	0,24	0,24	0,00	0,00
ErQpcc	0,00	0,00	0,00	0,00	0,08	0,08	0,09	0,44	0,44	0,88	0,88	0,00	0,00
ErIq	0,00	0,00	0,01	0,01	0,00	0,00	0,00	0,01	0,01	0,00	0,00	0,98	0,98
ErId	0,00	0,00	0,01	0,01	0,00	0,00	0,00	0,00	0,00	0,01	0,01	1,00	1,00
ErPLL	0,70	0,70	0,00	0,00	0,00	0,00	0,00	0,00	0,00	0,00	0,00	0,00	0,00
W	1,00	1,00	0,96	0,96	0,20	0,20	0,00	0,21	0,21	0,01	0,01	0,02	0,02

Figure 7.14: Participation Factors for fourth Value of τ_{pcc}. Case 3

Val.1	Mode1	Mode2	Mode3	Mode4	Mode5	Mode6	Mode7	Mode8	Mode9	Mode10	Mode11	Mode12	Mode13
f (Hz)	59,69	59,69	0,00	0,00	0,41	0,41	0,00	0,00	0,00	0,00	0,00	0,00	0,00
damp	0,42	0,42	1,00	1,00	0,21	0,21	1,00	1,00	1,00	1,00	1,00	1,00	1,00
FreqR1	0,00	0,00	0,00	0,00	0,73	0,73	0,26	0,63	0,01	0,06	0,00	0,00	0,00
FreqR2	0,00	0,00	0,00	0,00	0,23	0,23	1,00	0,17	0,00	0,05	0,00	0,00	0,00
FreqR3	0,00	0,00	0,00	0,00	1,00	1,00	0,12	0,07	0,00	0,00	0,00	0,00	0,00
Iq	0,28	0,28	0,85	0,85	0,00	0,00	0,00	0,00	0,00	0,00	0,00	0,02	0,02
Id	0,48	0,48	1,00	1,00	0,00	0,00	0,00	0,00	0,00	0,00	0,00	0,03	0,03
ErPz	0,04	0,04	0,03	0,03	0,21	0,21	0,00	0,61	0,03	1,00	0,55	0,00	0,00
ErQz	0,03	0,03	0,04	0,04	0,03	0,03	0,01	0,14	0,16	0,54	1,00	0,00	0,00
ErPpcc	0,00	0,00	0,00	0,00	0,36	0,36	0,00	1,00	0,10	0,19	0,08	0,00	0,00
ErQpcc	0,00	0,00	0,00	0,00	0,05	0,05	0,01	0,20	1,00	0,08	0,17	0,00	0,00
ErIq	0,00	0,00	0,01	0,01	0,00	0,00	0,00	0,00	0,00	0,00	0,00	1,00	1,00
ErId	0,00	0,00	0,01	0,01	0,00	0,00	0,00	0,00	0,00	0,00	0,01	1,00	1,00
ErPLL	0,74	0,74	0,00	0,00	0,00	0,00	0,00	0,00	0,00	0,00	0,00	0,00	0,00
W	1,00	1,00	0,90	0,90	0,03	0,03	0,00	0,06	0,00	0,02	0,00	0,02	0,02

Figure 7.15: Participation Factors for the first Value of τ_{pcc}. Case 3

quency. In this case the main variables participating are the current states and the angular speed state.

- Modes 5 and 6 are highly participated by the states of the Frequeny Response Model: FreqR1, FreqR2, FreR3. Also it can be seen in the frequency and dampening ratio that it involves very low frequency signal but with a very low dampening ratio, which matches with the kind of oscillation that the Frequency Response Model generates. Apart from this it can also be highlighted the error input from the active power PPC and the active power controller of the VSC. The link among these variables seems logic due to the link throughout the frequency droop.

- Mode 7 is a real mode where the states involved just belong to the Frequency Response Model.

- Mode 8 can also be related to the frequency droop control since the main variables participating are a state from the Frequency Response Model and the input error of the Active Power control of the PCC.

- Modes 9, 10 and 11 are non-oscillatory modes where the main states involved are the ones from the PPC and the active and reactive power controller. As well, in Modes 10 and 11 it can be seen the mutual interaction between the active power and reactive power states in the power converter controller.

- Modes 12 and 13 are two more non-oscillatory modes where only the error states from the current loop participate.

When comparing this results with the ones gathered in Figure 7.14 it can be seen that there are considerable differences. First of all, when looking at the oscillatory modes, it can be seen that the frequency in Modes 1, 2, 5 and 6 frequency and dampening ratio have increased. Apart from this it is very remarkable how Modes 10 and 11 have increased considerably their frequencies and dampening ratios and specially how modes 8 and 9 have turned from two independent non-oscillatory modes to two modes related to a conjugated pair of poles.

7.4.3 Time Domain

Time domain simulations have also been carried out in this case for all the different time constant considered. Converters voltage response is shown in Figure 7.16, PCC voltage are

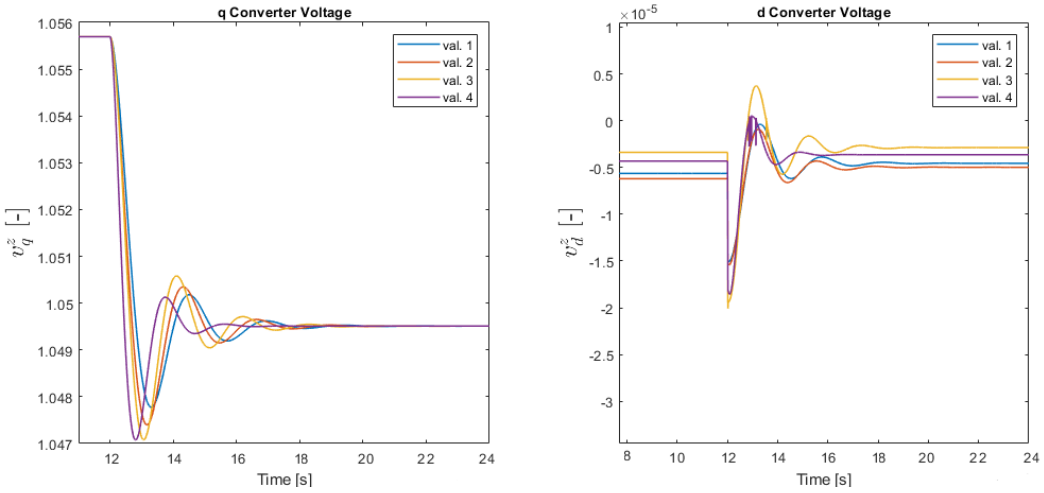

Figure 7.16: Comparison of converter's voltage responses. Case 3

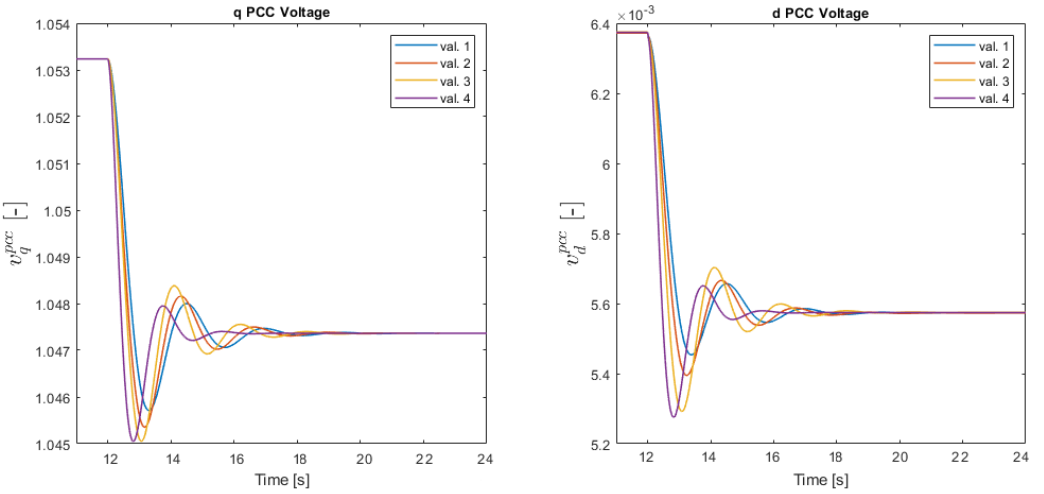

Figure 7.17: Comparison of voltage responses in PCC. Case 3

presented in Figure 7.17, currents are presented in Figure 7.18 and finally the powers responses are plotted in Figure 7.19. Looking at all the plots it can be seen how the dynamics are pretty similar for the first and second time constant value while the third and fourth value differ slightly from them. Besides it can be added how the typical frequency response oscillations are replicated in every variable, only differentiating from each other due to earlier and higher amplitude overshoots.

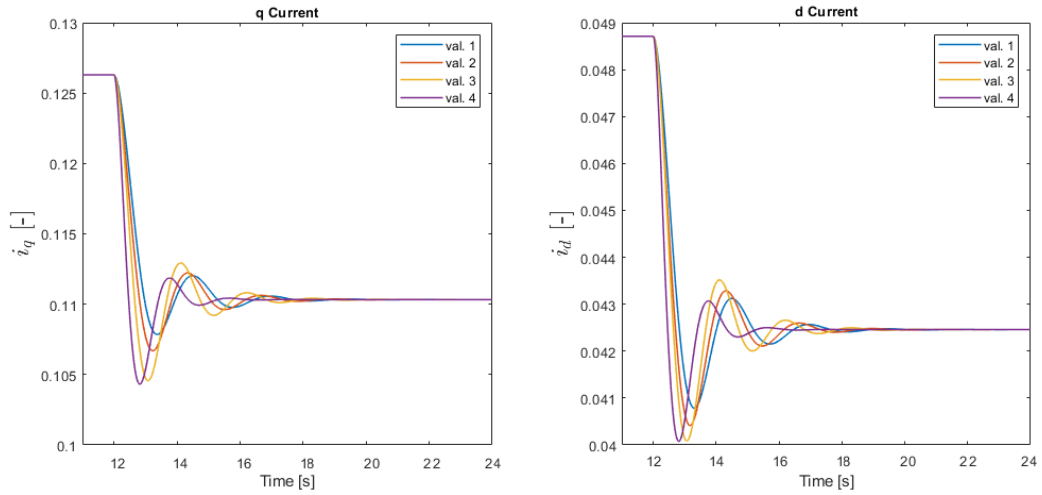

Figure 7.18: Comparison of current responses. Case 3

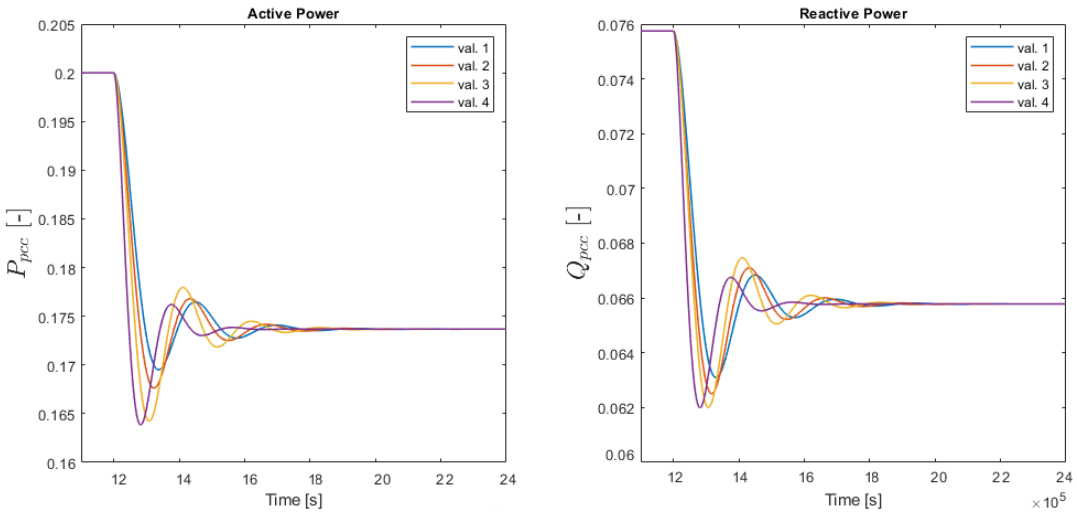

Figure 7.19: Comparison of power responses. Cases 3

7.5 Discussion

If the pole diagrams that have been built for the different cases are compared, two different regions can be differentiated to analyze the effect of the system's speed-up. When looking close to the origin it can be seen how the second and third case have several conjugated imaginary poles of very low frequency. In contrast, in the first case only poles with real negative part can be found. On the other hand, further away from the origin the results from case 1 and 2 are more similar since the location of a pair of conjugated poles barely changes, while it does a lot for the same pole in the third case.

With regard to the time domain simulations, the most remarkable feature to be mentioned is related to the fact that the dynamics barely vary with the time constant variation for every case considered. Despite initial hypothesis in which the time constant influence was considered to be a pivotal factor in the dynamics and stability of the system, the model that has been studied has not been able to find those kind of limitations. Likewise, this implicitly involves that the controllers design and control topology are more robust than it was previously thought in the case where further plant components are not considered.

As far as participation factors are concerned, it can be seen that for every case considered there is a common oscillating mode that in every set of participation factors holds the biggest frequencies and usually the lowest damping ratios. If the focus is put on this Mode, it can be seen how the PLL states, the PI error input and the angular speed calculation, are the main participators. However,it must be highlighted that the current states also participate up to certain point in this mode, becoming quite relevant in the third case where the d current state computes up to half of the main contributors participation. This is something to bear mind when defining the level of robustness of a PLLs if the current oscillations are intended to be minimized in a real scenario. When it comes to the non-oscillatory modes, some common trends can be highlighted. In every case the variables involved are related whether to the error states from both the PPC controllers and the active and reactive power controller of the converter, or the current controller states. This interaction makes sense due to the cascaded topology that links outputs and inputs from the different controllers. For the rest of the oscillating modes found, it can be seen that their influence is very limited since they are only disclosed for very small time constants and commonly with very low frequencies and high dampening ratios. In fact, it is very difficult to find those oscillations in the time domain simulations.

Chapter 8

Conclusions

This project has introduced the issue related to the impact of massive integration of renewable energy plants on the power system's stability and reliability. In relation to this phenomenon, new grid code developments have also been presented as an amendment for the incoming generation of large renewable plants where grid support is defined as compulsory. Thus, with the aim of studying the performance of this type of plant under such conditions, the typical control topology of a large PV power plant has been exposed, defining each subsystem and its working principles. Following this purpose, a non linear model of the PV power plant connection has been developed focusing on two different matters:

- Controllers design considering time response specifications
- Integration of different control modes operations related to different grid conditions: variable frequency and voltage.

Before applying linear control techniques that ease figuring out the main dynamic features of the system , the resulting non-linear model has been used to set the basis that has enabled the required development of a linear model. In this regard, a validation of the model's adequacy has been carried out for the three different control modes.

By means of the derived linear models, a dynamics analysis of the system has been carried out by performing a calculation of the eigenvalues of the model, time domain simulations and a modal analysis based on calculation of participation factors. The main outcomes from this analysis state that the systems stability is barely compromised by a considerable reduction of the power plant controller time constant. However, it has been proven that the

variable frequency case is featured by a bigger number of oscillating modes. In addition, in this scenario a considerable degree of interaction between currents and PLL performance as well as higher oscillation frequencies and lower damping ratios than the two other cases. This way, in order to avoid critical and undesired behaviours in the system such as the previous one involving the current, further study on variable frequency models with additional elements such as DC side of the converter, detailed transformer models or a number of VSC working together can be worth the effort to ensure future's grid reliability.

Appendix A

Budget

The present appendix presents the potential budget that the development of a project of this short would need.

The labour distribution from different activities is presented in the following table along the time cost and the total computed cost.

Task	Time Spent (hour)	Unit Cost (Euro/hour)	Total (Euro)
Research	100	40	4000
Development	300	40	12000
Writing	100	40	4000
Total	500	-	20000

Figure A.1: Labour Costs

If the costs of transport are considered, in this case it would mean 21 Euros per month of expenses considering public transport. Considering a 7 month length of work transport costs compute a total of 147 euros.

External consulting and advising is another source of expense when carrying out a research project of this kind. For this project experts advisory has been required.

External Services	Time Spent (hour)	Unit Cost (Euro/hour)	Total (Euro)
Consulting and Advisory	40	80	3200

Figure A.2: External services costs.

Finally the total costs sum up to: 23347 Euros.

Appendix B

Park transformation

The Park transformation is a tool used to turn an oscillatory three phase system in a DC or constant magnitudes system [15]. This feature is crucial for controls design since it eases the task, hence it is widely used in the field of electrical engineering.

The Park transformation is given by

$$[x_{qd0}] = T(\theta)[x_{abc}] \tag{B.1}$$

and inverse the inverse operation by

$$[x_{abc}] = T(\theta)^{-1}[x_{qd0}] \tag{B.2}$$

x_{abc} is a three phase vector in the abc frame, while x_{qd0} is the resulting vector after the transformation in the synchronous reference frame,usually reference as $dq0$ frame. θ on the other hand is a voltage angle used as reference. In a balanced system, the 0 component will be null. $T(\theta)$ is the Park transformation matrix, which is commonly defined with the following matrix:

$$T(\theta) = \frac{2}{3}\begin{bmatrix} cos(\theta) & cos(\theta - \frac{2\pi}{3}) & cos(\theta + \frac{2\pi}{3} \\ sin(\theta) & sin(\theta - \frac{2\pi}{3}) & sin(\theta + \frac{2\pi}{3}) \\ \frac{1}{2} & \frac{1}{2} & \frac{1}{2} \end{bmatrix} \tag{B.3}$$

Applying the inverse operation to this matrix:

$$T(\theta)^{-1} = \begin{bmatrix} cos(\theta) & sin(\theta) & 1 \\ cos(\theta - \frac{2\pi}{3}) & sin(\theta - \frac{2\pi}{3}) & 1 \\ cos(\theta + \frac{2\pi}{3}) & sin(\theta - \frac{2\pi}{3}) & 1 \end{bmatrix} \tag{B.4}$$

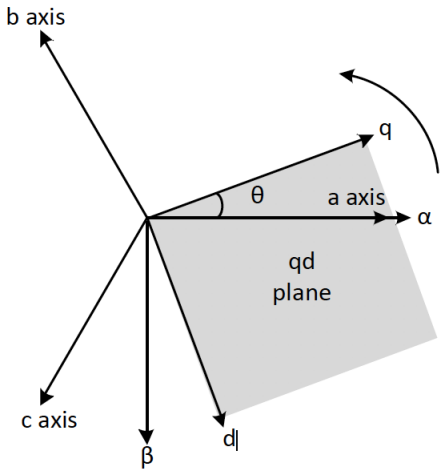

Figure B.1: qd plane representation

B.1 Clarke Transformation

Park transformation can be applied by carrying out an orthogonal transformation plus a rotation. This orthogonal transformation consists on placing three phase phasors spaced 120 degrees in a new reference plane where two of them form a 90 degrees and third one is perpendicular to such plan. This transformation is the so-called Clarke transformation, where electrical quantities are expressed in $\alpha\beta 0$ orthogonal reference frame. The null component is 0, α and β are two magnitudes 90 degrees shifted oscillatory nature.

Clarke's transformation and inverse matrix are expressed as the following:

$$T_{\alpha\beta 0} = \frac{2}{3}\begin{bmatrix} 1 & -\frac{1}{2} & -\frac{1}{2} \\ 0 & -\frac{\sqrt{3}}{2} & \frac{\sqrt{3}}{2} \\ \frac{1}{2} & \frac{1}{2} & \frac{1}{2} \end{bmatrix} \tag{B.5}$$

$$T^{-1}_{\alpha\beta 0} = \begin{bmatrix} 1 & 0 & 1 \\ -\frac{1}{2} & -\frac{\sqrt{3}}{2} & 1 \\ -\frac{1}{2} & \frac{\sqrt{3}}{2} & 1 \end{bmatrix} \tag{B.6}$$

Appendix C

Environmental Impact

This appendix sumarizes the imapct that large photovoltaic power plants can have in the environment and some other issues related to the development of similar projects in the industry.

One of the main problems related to the integration of large PV power plant is the vast occupation of land that it involves. In some cases this can go together with forest and rainforest deforestation, and thus natural habitat loss that directly impacts on the autochthonous wildlife. In this regard it must also be mentioned the potential occupation of farmland that can reduce the amount of available agricultural produces leading to the rise of food in local markets. An alternative in this sense is the installation of PV modules in the rooftops.

Another point related to the impact of these projects has to do with the materials used to made up the different power plant elements. Iron, copper, aluminium and other similar materials are more extensively used than in other kinds of power plants which implicitly involves further impact on mining regions.

In addition to the previous mentioned metallic elements e nitric acid, sulphuric acid and acetone are hazardous products used in the modules and inverters, that in case of not proper after treatment can have considerable impact on whatever ecosystem they land on.

Bibliography

[1] R. Iravani A. Yazdani. *Voltage-Sourced Converters in Power Systems: Modeling, Control, and Applications*. Wiley-IEEE Press, 2010.

[2] Yang Chen et al. Allen M. Mustafa Babiker M. *Global warming of 1.5°C*. Intergovernmental Panel on Climate Change, 2015.

[3] Adriá ; Gomis-Bellmunt Oriol gea Alvarez Agustí ; Junyent-Ferré. *Active and Reactive Power Control of Grid Connected Distributed Generation Systems. Modeling and Control of Sustainable Power Systems: Towards Smarter and Greener Electric Grids*. Springer, 2012.

[4] Monica Aragues-Penalba-Oriol Gomis-Bellmunt Ana Cabrera-Tobar Eduard Bullich-Massague. "Review of advanced grid requirements for the integration of large scale photovoltaic power plants in the transmission system". In: (2016).

[5] Bjarne W.; Thorsen Jan Eric; Svendsen-Svend Brand Marek; Olesen. *COMMISSION REGULATION (EU) 2016/631*. Official Journal of the European Union, 2016.

[6] Eduard Bullich-Massagu. *Feeder ow control and operation in large scale photovoltaic power plants and microgrids*. Universitat Politècnica de Catalunya, 2016.

[7] Se-Kyo Chung. "A phase tracking system for three phase utility interface inverters". In: (May 2000.).

[8] F. Liu K. Xin Y. Liu D. Yang X. Wang and F. Blaabjerg. "Impedance shaping of the grid-connected inverter with LCL filter to improve its adaptability to the weak grid condition," in: (2017).

[9] E. H. Watanabe H. Akagi and M. Aredes. "Instantaneous power theory and applications to power conditioning". In: (2007).

[10] IRENA. *Renewable capacity highlights*. International Renewable energy Agency, 31 March 2018.

[11] Montero J. "Interaction analysis of large-scale PV power plants considering the AC network". In: (2018).

[12] Tchung-Ming S. Diaz-Vazquez A. R. Weitzel M.-Vandyck T. Després J. Schmitz A. Rey Los Santos L. Wojtowicz K. Schade B. Saveyn B. Soria-Ramirez A. Keramidas K. *Global Energy and Climate Outlook 2018: Sectoral mitigation options towards a low-emissions economy*. Joint Research Centre for Policy Report, European Comission, 2018.

[13] V. Konoval and R. Prytula. "Participation Factor in Modal Analysis of power systems stability". In: (2016).

[14] P. Kundur. *Power System Stability and Control*. McGraw-Hill Education, 1994.

[15] R. H. Park. "Abridgment of two-reaction theory of synchronous machines generalized method of analysis — Part I". In: (2008).

[16] Fang Zheng Peng and Jih-Sheng Lai. "Generalized instantaneous reactive power theory for three-phase power systems". In: (1996).